

Sustainable Silicon-Containing Resources Utilization and Performance Optimization of Silicon-Based Anode Materials

Zihong Yu, Xinlin Peng, Jie Liu, Qiangchao Sun,* Zhifeng Xu, Weifan Gao, and Hongwei Cheng*



Silicon (Si) is a highly promising anode material for next-generation lithium-ion batteries due to its ultra-high theoretical specific capacity (4200 mAh g^{-1}), abundant reserves, and suitable working voltage. However, its industrialization is hindered by the high cost of nanosilicon, significant volume expansion, and low electrical conductivity, necessitating sustainable silicon sources that are cost-effective and environmentally friendly. Compared to high-purity nanosilicon, biomass silicon, mineral silicon, and industrial waste silicon serve as alternative silicon sources that not only effectively reduce the production costs of silicon-based anodes but also alleviate resource scarcity and environmental pollution. This review summarizes the resource characteristics,

development potential, and key technologies for preparing nano-silicon from these three types of low-cost silicon sources. Furthermore, it highlights optimization mechanisms for enhancing the electrochemical performance of silicon anodes through modification strategies such as carbon composite design, atomic doping, and hierarchical structure construction. By integrating a multidimensional approach encompassing three parts: resource screening, controllable preparation, and synergistic modification, this work aims to advance silicon-based anode materials, providing economically viable and eco-friendly solutions for advanced lithium-ion batteries and promoting the development of sustainable electrochemical energy storage technologies.

1. Introduction

The rapid advancement of metal-ion battery systems is witnessing particularly strong growth in the lithium-ion battery market, which serves as a critical enabler for energy transition and low-carbon development.^[1–3] Industry projections indicate that this market will surpass \$5.12 trillion by 2034, fueled primarily by surging demand from electric vehicles, grid-scale energy storage, and evolving consumer electronics.^[4–6] However, the current dominance of graphite anodes, with their intrinsic limitation of a low theoretical capacity (372 mAh g^{-1}), fails to meet escalating energy density requirements.^[7,8] This critical gap has positioned silicon-based anodes as the most promising next-generation solution, owing to their exceptional theoretical capacity (4200 mAh g^{-1} in a form of $\text{Li}_{22}\text{Si}_5$ at room temperature, ≈ 10 times that of graphite), terrestrial abundance, and suitable operating voltage (0.2–0.3 V vs Li/Li⁺).^[9–12] Nevertheless, the commercialization timeline for next-generation high-energy-density batteries remains contingent upon resolving fundamental challenges in silicon anode technology.^[13]

Industrial-scale adoption faces two primary constraints. First, prohibitive production costs: current reliance on high-purity nanosilicon (>99.9%) necessitates expensive, energy-intensive processes such as the chemical vapor deposition (CVD) technique, rendering silicon anodes economically uncompetitive against graphite.^[14,15] Notably, prevailing research exhibits a

significant oversight, while extensive efforts focus on nanosilicon modification strategies, most reviews neglect the foundational issue of silicon feedstock economics and sustainable sourcing. Analyses by the Lassi team primarily focus on composite synthesis methodologies, whereas Yu et al. emphasize microsilicon structural optimization—yet both neglect systematic assessment of cost-effective silicon sources.^[16–18] Therefore, the economic viability and environmental sustainability of silicon feedstocks are essential to enable the transition of advanced academic research, particularly in high-performance silicon-based anode materials, into scalable and commercially feasible industrial applications.

Moreover, silicon-based materials still suffer from two inherent defects. First, severe intrinsic resistivity ($10^3 \Omega \text{ cm}$) severely impedes charge transfer kinetics, degrading rate capability and cycle life.^[19,20] Secondly, silicon undergoes extreme volume expansion, with over 300% during lithiation, which leads to particle pulverization and triggers continuous rupture and reformation of the solid electrolyte interphase (SEI).^[21–23] This parasitic process depletes lithium inventory, increases internal resistance, and accelerates capacity fading. Thereby, holistic mitigation of these defects is paramount for achieving long-term electrochemical stability.^[24] At present, researchers have developed modification strategies such as carbon compositing,^[25–27] heteroatom doping,^[28–30] and structural engineering,^[31–33] which have demonstrated efficacy in enhancing conductivity and buffering volume changes. However, current research exhibits a structural imbalance characterized by “flourishing modifications but stagnant source innovation.” A critical gap exists in integrating low-cost silicon resources (e.g., rice husks, photovoltaic waste) with subsequent performance optimization strategies. Therefore, addressing this necessitates a synergistic innovation model bridging resource valorization with anode engineering.^[34]

Low-cost silicon sources offer the advantages of abundant reserves, low cost, and environmental friendliness. Their unique structural features can effectively mitigate volume expansion in silicon-based anodes while promoting sustainable development through resource recycling. For example, porous silicon derived from rice husks^[35] delivers a remarkable residual capacity exceeding 760 mAh g^{-1} after 300 cycles, while bamboo charcoal-based^[36] silicon–carbon composites combine cost-effectiveness,

Z. Yu, X. Peng, J. Liu, Q. Sun, H. Cheng
School of Materials Science and Engineering & State Key Laboratory of Advanced Refractories
Shanghai University
Shanghai 20444, China
E-mail: qiangchao_sun@shu.edu.cn
hwcheng@shu.edu.cn

Z. Xu
Key Laboratory of Ionic Rare Earth Resources and Environment, Ministry of Natural Resources
Jiangxi College of Applied Technology
Ganzhou, Jiangxi 341000, China
W. Gao
Jiangxi Silicon Ore Utilization Core Technology R&D Investment Co., LTD
Ji'an, Jiangxi 343999, China

eco-friendliness, and scalability, achieving a reversible capacity of 603 mAh g^{-1} at 200 mA g^{-1} for 120 cycles. Mineral silicon sources, such as vermiculite,^[37] exhibit abundant reserves and structural stability; their naturally layered porous nanosheets facilitate charge transport, electrolyte infiltration, and volume expansion accommodation. Industrial waste silicon, particularly photovoltaic kerf,^[38] stands out for its high purity and low cost, with recycled silicon anodes retaining a capacity of 1010 mAh g^{-1} after 148 cycles at 0.5 A g^{-1} . Collectively, these sustainable silicon sources not only mitigate production costs but also align with circular economy principles, demonstrating significant potential for next-generation silicon-based anodes.

To comprehensively analyze these interconnected challenges, this review establishes an integrated framework “from silicon resources, controllable preparation, and multiple modifications to application orientations”, as exhibited in **Figure 1**. We systematically evaluate three major categories of low-cost silicon precursors: biomass-derived, mineral-based, and industrial waste streams,^[39] while elucidating key technological pathways for their conversion into battery-grade silicon. Furthermore, we conduct a comprehensive analysis of modification strategies, examining how structural design, compositional tuning, and morphological control regulate critical performance parameters (conductivity, volume expansion suppression, cycling stability) of silicon-based anodes. By linking resource characteristics with end-use application demands, this work provides a systematic blueprint for developing high-performance, low-cost, and sustainable silicon-based anodes, thereby accelerating their industrial implementation.



Zihong Yu is a master's student in the School of Materials Science and Engineering of Shanghai University, supervised by Prof. Hongwei Cheng. She received her B.S. degree from Jiangxi University of Science and Technology in 2024. Her main research interests focus on the design of advanced silicon-based anode materials for lithium-ion batteries.



Xinlin Peng is currently pursuing her Master of Science degree under the supervision of Prof. Hongwei Cheng at the School of Materials Science and Engineering, Shanghai University, China. She received her B.S. degree from Jiangxi University of Science and Technology in 2024. Her research interests focus on the design of advanced silicon-based anode materials for lithium-ion batteries.



Jie Liu is currently a Ph.D. degree student under the supervision of Prof. Hongwei Cheng at the School of Materials Science and Engineering, Shanghai University, China. He received his B.S. degree from Jiangxi University of Science and Technology in 2024. His research interests focus on the design of composite solid-state electrolytes and ternary cathode materials for all-solid-state lithium-ion batteries.

2. Low-Cost Silicon-Containing Resources

2.1. The Roadmaps of Silicon-Based Anodes

Silicon-based anodes are crucial for next-generation batteries but face commercialization barriers from cycling volume expansion and capacity degradation. The key developmental milestones of silicon-based anodes are depicted in **Figure 2**. Early studies confirmed silicon's lithium alloying behavior (forming $\text{Li}_{22}\text{Si}_5$) with a lower potential than graphite, yet volume management strategies were absent.^[40] As the research on silicon materials deepened, researchers discovered that the volume expansion range of silicon could be restricted by reducing its size to the nanoscale. In 2007, Cui et al. fabricated silicon nanowire electrodes, leveraging nanoscale dimensions to accommodate strain. This inspired research on nanoparticles and nanosheets.^[41] In 2011, Gleb et al. built high-capacity Si nanopowder-based lithium-ion batteries and mentioned that the capacity of silicon is more than one order of magnitude higher than that of graphite.^[42] However, the nanoscale surfaces made the SEI more unstable.^[43] Subsequently, porosity engineering has garnered significant attention due to its ability to buffer volume expansion through the inherent porosity within the material. For instance, in 2013, Zhou et al. developed chemically etched porous silicon, utilizing intrinsic voids to buffer expansion while mitigating SEI issues inherent to nanomaterials.^[44] Meanwhile, the flexibility of carbon materials can be employed to mitigate volume expansion, which has spurred the development of silicon–carbon (Si/C) composite anode materials.



Qiangchao Sun is an associate researcher in the School of Materials Science and Engineering of Shanghai University. He obtained his Ph.D. degree in metallurgical physical chemistry from Shanghai University in 2022 under the supervision of Prof. Hongwei Cheng. He conducted postdoctoral research at Shanghai University in the field of battery chemistry from 2022 to 2025. His research interests focus on advanced materials and technologies for lithium-ion batteries and aqueous metal batteries.



Hongwei Cheng is a professor of metallurgical physical chemistry at the School of Materials Science and Engineering, Shanghai University. He received his Ph.D. in Metallurgical Engineering from Shanghai University in 2009 and worked as a visiting scholar at the University of Wisconsin-Madison from 2018 to 2019. His primary research focuses on the development of cutting-edge materials and their application in electrochemical energy conversion and storage systems, including electrodes and electrolytes for lithium-ion batteries, electrode materials/electrolytes for aqueous secondary batteries, as well as oxygen-permeable membranes for hydrogen production.

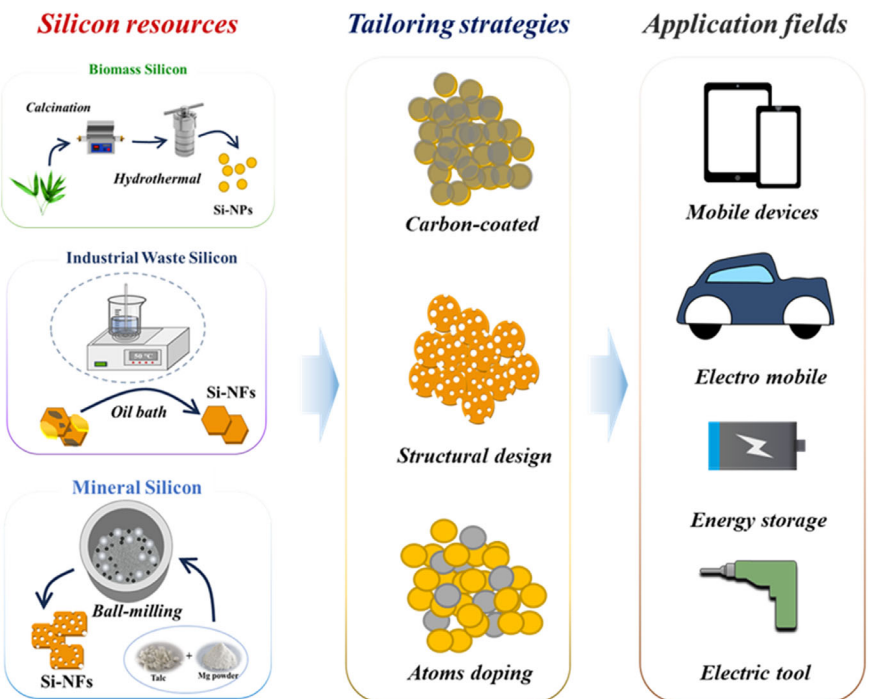


Figure 1. A four-dimensional framework of resources–preparation–modification–application.

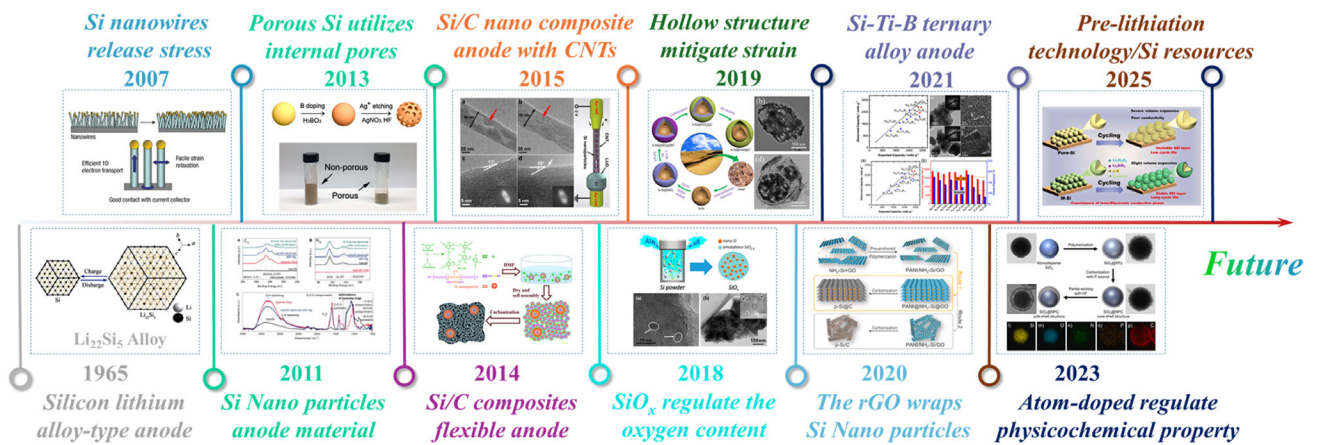


Figure 2. The advancement of Si-based anode materials for lithium-ion battery.

The listed carbon hybridization advancements in here including: conductive networks, integration of carbon nanotubes (CNTs), established flexible “Si-CNT” architectures, enhancing electron transport, and strain tolerance.^[45,46] Yolk-shell structures: Xie et al. synthesized Si@Void@C microspheres via low-temperature aluminothermic reduction, where carbon shells and internal cavities synergistically stabilized cycling. Graphene integration: in 2000, Tang et al. employed reduced graphene oxide (rGO) encapsulation, exploiting its high conductivity and large surface area to improve interfacial kinetics.^[47,48] As silicon–carbon composites are developing rapidly, silicon oxides have attracted attention due to their low cost and high first Coulombic efficiency.^[32] In 2018, Obrovac et al. studied the performance of such anode

materials by altering the oxygen content in the SiO_x material.^[49] Furthermore, researchers have tried to dope other atoms into silicon-based materials and found that doping silicon or carbon layers with nonmetallic (N, P, S) or metallic (Al, Mg) atoms can effectively modulate the electronic structure, surface activity, and interfacial stability, thereby optimizing ion intercalation/deintercalation behavior. In 2021, Peng et al. prepared a Si-Ti-B ternary alloy anode and achieved stable cycling of high-energy-density lithium-ion batteries by adjusting the inactive phase in the Si-Ti-B ternary alloy anode.^[50] In 2022, Baeck et al. implemented N, P co-doping in carbon shells, simultaneously optimizing electronic conductivity and lithium storage capacity through tailored electronic structures.^[29] Recently, to

address the key issue of low initial Coulombic efficiency during the cycling of silicon-based materials, a prelithiation technique has been developed. Huang et al. engineered *in situ* prelithiation protocols to construct ion/electron-conductive interfaces, significantly boosting initial Coulombic efficiency and cycle life.^[51] Despite progress, high silicon material costs impede mass adoption. By exploring and optimizing the preparation process of low-cost silicon sources, it is feasible to further reduce the production costs of silicon-based anodes. This would facilitate their extensive application in energy storage systems and lay a solid foundation for the commercial development of high-performance and cost-effective lithium-ion battery technologies. Recently, propelled by the exponential growth of the new energy and semiconductor sectors, the soaring demand for silicon has led to a continuous upward trend in silicon prices. This tendency is especially evident in the nanosilicon segment. Here, complex synthesis procedures—frequently involving high-energy ball milling, CVD, or laser ablation—along with strict purity requirements significantly increase production costs. As a result, the high cost of nanosilicon has become a major obstacle to the wide commercialization of high-energy-density silicon-based anodes in lithium-ion batteries. This economic situation highlights the crucial necessity of developing and utilizing alternative, cost-efficient Si sources that can be directly incorporated into anode manufacturing processes without sacrificing electrochemical performance. Strategically, as shown in **Figure 3**, these alternative silicon sources can be mainly classified into three categories (biomass silicon, mineral silicon, and industrial waste silicon) according to their origin and inherent structural attributes.

2.2. Biomass-Derived Silicon Source

Biomass-derived silicon, extracted from silica-rich biological sources such as rice husks, reeds and bamboo leaves, demonstrates compelling advantages, including sustainable availability, low-carbon footprint, and environmental compatibility. In these plant-based materials, silicon predominantly exists as amorphous

silica (SiO_2) within structural components like stems and leaves. Critically, this biomass-hosted SiO_2 inherently possesses hierarchical porous architectures.^[52] When preserved during conversion to elemental silicon, these intrinsic pore networks create vital void spaces that effectively accommodate the volume expansion of silicon anodes during electrochemical cycling, thereby mitigating mechanical degradation.^[53] The global abundance of such resources is substantial, exemplified by annual rice husk production exceeding 100 million tons—a high-yield agricultural byproduct whose ash contains 15–20 wt% SiO_2 . Moreover, transforming these residues into high-value silicon anode materials aligns perfectly with China's low-carbon and green development principles.^[54]

Rice husks represent a highly promising biomass silicon source, primarily composed of lignin, cellulose, hemicellulose and ≈20 wt% SiO_2 . This substantial SiO_2 content positions rice husks as an ideal precursor for silicon-based materials.^[55] Processing methodologies capitalize on dual functional pathways: controlled calcination concurrently transforms embedded organic matrices (e.g., lignin/cellulose in rice husks) into conductive carbon layers while converting SiO_2 to active silicon. This *in situ* carbon modification yields electrochemically optimized Si/C composites without requiring separate conductive additives.^[56] Moreover, bamboo leaves, as another viable biomass silicon source, naturally contain silicon predominantly in the form of SiO_2 , where the content varies significantly depending on bamboo species and growth environment. Bamboo leaves exhibit species-dependent silica distribution and a distinctive tubular microstructure that enhances electrode mechanical integrity and ion diffusion kinetics upon conversion.^[57] Similarly, as widely distributed perennial grasses, reeds accumulate significant silica through natural soil silicate assimilation, with their preserved three-dimensional (3D) nanostructures, which effectively buffer volume expansion during cycling, improving cycling stability in derived anodes.^[58]

Beyond these primary sources, oat husks, diatoms, and cabbage leaves represent supplementary silica-rich biomass reservoirs suitable for anode material synthesis. Environmentally, repurposing agricultural waste for high-value silicon production directly addresses the ecological damage caused by open burning while aligning with circular economy principles and national green development strategies, transforming disposal challenges into technological opportunities.^[59–61]

2.3. Silicon-Containing Mineral Resources

Unlike biomass silicon, mineral silicon offers geological abundance and structural stability, making it a scalable option for industrial applications. Mineral silicon, derived from naturally abundant silicon-bearing minerals and rocks, predominantly exists as SiO_2 or silicates rather than elemental forms, with common sources including diatomite, montmorillonite, and natural quartz sand.^[62] As anode precursors, these mineral sources offer compelling advantages: inherent low cost, high geological purity, and exceptional structural stability. Critically, their utilization



Figure 3. Schematic diagram of the classification of low-cost silicon sources.

bypasses complex synthesis routes required for gaseous (SiH_4) or liquid (TEOS) silicon precursors. Furthermore, many exhibits innate nanostructures—such as nanotubular arrays, layered nanosheets, and interconnected porous networks—that can be topochemically converted into engineered silicon nanomaterials (e.g., porous silicon) while preserving beneficial architectures. These intrinsic nanochannels provide high specific surface areas conducive to rapid Li^+ diffusion kinetics.^[63]

Diatomaceous earth, a biogenic mineral composed of fossilized diatom skeletons, presents as a lightweight white/gray powder with 85–94% amorphous SiO_2 content.^[64] Its unique honeycomb microstructure delivers ultrahigh surface area and open porosity, while the amorphous silica's enhanced reactivity enables energy-efficient reduction compared to crystalline quartz.^[65] Although naturally containing minor impurities (2–5 wt% Al/Fe oxides), these are readily removable via selective acid leaching. Crucially, diatomite's natural porous framework serves as a self-supporting template, eliminating the need for high-temperature crystallization treatments. Montmorillonite, a layered aluminosilicate clay, features a 2:1 tetrahedral-octahedral-tetrahedral sandwiching structure.^[66] When subjected to integrated reduction-exfoliation processes, its interlayer cations (e.g., Mg^{2+} , Al^{3+}) act as *in situ* thermal buffers during magnesiothermic reduction, suppressing particle agglomeration while directing the formation of mechanically robust two-dimensional (2D) silicon nanosheets. Natural quartz sand, primarily comprising >98% crystalline quartz (SiO_2) with trace $\text{Fe}_2\text{O}_3/\text{Al}_2\text{O}_3$ impurities, leverages its highly ordered silicon–oxygen tetrahedral structure for exceptional chemical stability. For anode applications, it typically undergoes high-energy ball milling combined with molten salt-assisted reduction to yield active silicon particles.^[67,68] Additional mineral sources like vermiculite, kaolin, and talc powder further expand the structural and chemical diversity available for silicon anode development. Collectively, these mineral-derived silicon precursors provide not only abundant, low-cost raw materials but also structurally versatile templates for high-performance anode engineering.^[69,70]

2.4. Industrial Secondary Silicon-Containing Resources

While biomass and mineral silicon provide sustainable, scalable solutions for silicon-based anodes, industrial waste silicon offers an equally promising alternative by repurposing these high-purity byproducts into valuable materials, simultaneously addressing resource scarcity and advancing circular economy principles.^[71,72] These materials exhibit substantial silicon content (kerf sludge, >90% Si) yet require purification due to contaminant inclusions (Fe, Al, Ca, B, P) that impede direct anode application.^[73] Silicon kerf sludge, generated during wafer slicing processes, comprises high-purity monocrystalline silicon fragments (50–300 nm), silicon carbide abrasives, and organic cutting fluids. With global photovoltaic production yielding over 200,000 tons annually, this resource demands efficient reclamation. Prior to anode utilization, acid washing removes metallic impurities (Al, Ag, Pb), while subsequent ball milling achieves requisite

nanization.^[74] Coal fly ash, captured from coal-fired power plant emissions, contains amorphous aluminosilicate within hollow glass microspheres—a potentially massive silicon reservoir. Its amorphous SiO_2 and Al_2O_3 composition offers higher reactivity than crystalline quartz, enabling lower-energy reduction. Crucially, ≈80% of fly ash particles serve as self-supporting templates, while their inherent 5–15 wt% unburned carbon can be pyrolyzed *in situ* to form conductive networks.^[75,76] Industrial slurries—including semiconductor polishing solutions and etching wastes—contain 5–15 wt% solid content as colloidal nanosilica sol dispersed with metal salts and organics. Though exhibiting excellent colloidal stability from surface charge effects, these slurries necessitate purification to eliminate trace metals (Cu, Ni).^[77,78] Additional silicon-rich waste streams, such as discarded liquid crystal display (LCD) glass, windshield glass, and end-of-life photovoltaic panels, further expand this resource base, all requiring tailored purification protocols. Strategically, advancing these low-cost silicon sources through integrated impurity management and structure-preserving conversion represents a vital pathway toward economically viable silicon-dominant anodes, transforming industrial waste into high-performance battery materials while supporting circular economy objectives in electronics manufacturing.^[79,80]

The strategic development and optimization of low-cost silicon sources, spanning biomass derivatives, mineral precursors, and industrial waste streams, coupled with advanced material engineering solutions to address their inherent limitations, constitute an indispensable pathway toward economically viable silicon-dominant anodes. **Table 1** summarizes and compares three different types of silicon sources. By implementing tailored impurity management protocols, leveraging inherent material architectures (e.g., diatomite's porosity), and *in situ* modifications, which enable the production of anode materials that simultaneously satisfy electrochemical requirements and cost targets. This holistic resource-to-device paradigm not only circumvents the prohibitive expenses of high-purity nanosilicon synthesis but also transforms waste valorization into a competitive advantage.

3. Controlled Preparation of Nanoscale Silicon

Nanosilicon materials have emerged as a research hotspot in the field of advanced materials due to their unique quantum size effect, surface effect, and exceptional electrochemical properties. The utilization of low-cost silicon sources, including biomass silicon, mineral silicon, and industrial waste silicon, for the preparation of nanosilicon materials not only significantly reduces production costs but also enables high-value utilization of waste materials, which holds substantial significance for promoting green manufacturing and the development of a circular economy. However, the key to achieving this objective lies in the development of efficient and controllable silicon preparation technologies. Consequently, this section systematically summarizes the primary methods for preparing high-performance silicon-based anode materials (particularly for lithium-ion battery

Table 1. Summary of the performances of typical silicon sources.

Classification	Silicon source	Form of silicon	Preparation controllability	Advantages	Disadvantages	References
Biomass silicon	Rice husk	SiO ₂	Improve the compatibility of the substrate.	1. Environmentally friendly. 2. With sustainable silicon containing resources. 3. It has potential for natural carbon coating.	1. Impurities (such as K, Na, etc.) are difficult to remove completely. 2. Uneven particle size: Agglomeration is likely to occur during preparation.	[54]
	Bamboo leaves	SiO ₂	Construct three-dimensional networks.			[57]
	Reed	SiO ₂	Prone to generating microcracks.			[58]
	Oat husk	SiO ₂	Prevent agglomeration.			[59]
	Diatom	SiO ₂	Optimize the etching process.			[60]
Mineral silicon	Cabbage leaves	SiO ₂	Prevent structural collapse.			[61]
	Talc	[SiO ₄] ⁴⁻	Highly controllable layered structure.	1. Relatively high purity. 2. The preparation process is well-established. 3. The microstructure of the anode is controllable.	1. Nonrenewable. 2. High consumption for purification. 3. Ecological environment pressure for separation.	[63]
	Diatomite	SiO ₂	The structural fragility.			[64]
	Montmorillonite	[SiO ₄] ⁴⁻	The high specific surface.			[66]
	Natural sand	SiO ₂	The impurity content fluctuates greatly.			[67]
	Vermiculite	SiO ₂	Customize pore diameters.			[69]
Industrial waste silicon	Kaolinite	SiO ₂	The sheet-like form has high controllability.			[70]
	Cutting waste	Si	Remove the surface oxide layer.	1. Low-cost resources. 2. High silicon content. 3. Reduces the emission of industrial solid waste.	1. The purification process is complex and costly. 2. Significant performance fluctuations. 3. The supply depends on the upstream industry.	[71]
	Fly ash	SiO ₂	Removed unburned carbon.			[76]
	Waste sludge	Si	The formation of the glass phase.			[77]
	LCD glass	SiO ₂	Mechanically ground into nanopowder.			[79]
Windshield	SiO ₂	Precise control of the corrosion time.				[80]

anodes) with a focus on low-cost silicon sources. Figure 4 provides a simplified illustration comparing different methods for the synthesis of nanosilicon.

3.1. Preparation Method of Biomass Silicon Sources

Biomass silicon has emerged as a premium raw material for the synthesis of nanosilicon due to its high content of amorphous SiO₂ (up to 15–20 wt%), coupled with its renewable nature, abundant reserves, and cost-effectiveness. Its distinctive microstructure and porous characteristics provide favorable conditions for the fabrication of nanosilicon with specialized morphologies. The prevalent methodologies for synthesizing nanosilicon from biomass silicon sources encompass hydrothermal synthesis, mechanochemical reduction, metallothermic reduction, and molten salt methods.

The hydrothermal method leverages a high-temperature, high-pressure aqueous environment to facilitate the dissolution and reconstruction of biomass silicon. A representative process involves calcining biomass feedstock (e.g., rice husks) at 500–800 °C to eliminate organic compounds, yielding biomass ash rich in amorphous silica. Subsequently, the ash is blended with



Figure 4. Schematic diagram of the preparation of nanosilicon from biomass silicon, mineral silicon, and industrial waste silicon.

reducing agents (such as magnesium powder, glucose, or urea) in specific proportions, followed by the addition of deionized water to adjust the solid-to-liquid ratio. The mixture is then subjected to a hydrothermal reaction in an autoclave at 180–250 °C for 6–48 h. Postreaction, the product undergoes centrifugation, washing, and drying to yield nanosilicon material. Sudarman et al.^[81] successfully synthesized spherical silicon particles with an average diameter of ≈20 nm from rice husk via a 10 h hydrothermal reaction at 180 °C. Furthermore, by modulating the proportion of the reducing agent, mesoporous silicon materials with pore sizes ranging from 1.69 to 8.30 nm were obtained. The hydrothermal method offers the advantage of relatively mild reaction conditions and the ability to control particle size and morphology by adjusting parameters such as reducing agent ratio, reaction temperature, and duration. However, this method is constrained by prolonged reaction cycles and low yield.

The metallothermic reduction represents the most conventional approach for synthesizing nanosilicon from biomass-derived silicon, utilizing reactive metals (e.g., Mg, Al) to reduce SiO₂ at high temperatures. Typically, calcined biomass ash is uniformly mixed with a reducing agent at a mass ratio ranging from 1:0.8 to 1:2, with the addition of a small quantity of sodium chloride or calcium chloride as a fluxing agent. Subsequently, the mixture is heated to temperatures between 650–750 °C in an argon atmosphere for a reaction duration of 2–4 h. Upon completion of the reaction, the product is pulverized, and by-products are removed through hydrochloric acid treatment. Unreacted silicon dioxide is etched using hydrofluoric acid. The final nano silicon is obtained through washing and drying processes. Su et al.^[111] employed the aluminothermic reduction method to convert corn leaves into nanosilicon, preserving the high porosity and mixed amorphous/crystalline structural characteristics of the natural corn leaf template, thereby achieving exceptional electrochemical performance. The metallic thermal reduction method offers significant advantages, including thorough reaction completion and high yield, making it suitable for large-scale production. However, this method necessitates high-temperature conditions, and the acid-washing process generates substantial wastewater, posing certain environmental concerns.

Mechanochemical reduction represents a solid-state reaction methodology facilitated through mechanical force. Specifically, this technique involves the proportional mixing of biomass silicon sources with reducing agents, followed by mechanical grinding under inert atmosphere protection. The mechanical energy generated during the grinding process initiates the reduction reaction. The ball-milled products require subsequent purification to eliminate by-product magnesium oxide and unreacted silicon dioxide, ultimately yielding nanosilicon after washing and drying. Cho's research team employed planetary ball mills and industrial-grade grinding equipment to convert rice husk ash into highly crystalline porous silicon materials by triggering magnesium thermal reduction during mechanical collisions.^[82] This process overcomes the high-temperature limitations inherent in traditional magnesium thermal reduction methods, offering a uniform local reaction environment that mitigates impurity formation. The methodology demonstrates operational simplicity and low

equipment requirements, enabling the production of nanosilicon with varying particle sizes through the regulation of ball milling duration and ball-to-material ratio, though product purity remains significantly influenced by raw material quality.

The molten salt method constitutes a chemical reaction technique conducted within molten salt media. Typically employing low-melting-point multicomponent salt systems (such as NaCl-KCl or LiCl-KCl eutectic systems) as reaction media, this process involves mixing biomass ash with reducing agents in crucibles, followed by reaction at 200–500 °C for 2–4 h. Postreaction, the cooled products undergo water washing and acid treatment to obtain nanosilicon. Tao et al. utilized a CaH₂-AlCl₃ reduction system to fabricate spherical silicon nanoparticles with diameters ranging from 70 to 100 nm from rice husks at a low temperature of 200 °C.^[83] The molten salt method generally operates at temperatures 100–200 °C lower than conventional metal thermal reduction processes, yielding products with uniform particle size distribution. However, this approach presents challenges in molten salt recovery and elevated production costs.

3.2. Processing of Mineral Silicon Sources

Transitioning from biomass to mineral silicon sources, the focus shifts to abundant geological reserves and well-established extraction processes. While mineral silicon offers high purity and structural stability, its conversion into nanosilicon requires tailored methods to address energy consumption and impurity management. Mineral silicon primarily refers to silicate minerals (e.g., talc and montmorillonite) and quartz sand, which are widely distributed in nature. Its advantages lie in its abundant reserves, low extraction costs, and a silicon dioxide content typically ranging from 50 to 90% (with quartz sand approaching 99%). Mineral silicon serves as a raw material to produce nanosilicon, with common methods including the molten salt method, metallothermic, and mechanochemical reduction.

The metallothermic reduction process of mineral silicon typically comprises three primary stages: raw material pretreatment, high-temperature reduction, and acid washing with passivation treatment. Natural silicon minerals, characterized by their large particle size and low specific surface area, significantly increase the complexity of subsequent material processing. Consequently, during the pretreatment phase, it is essential to precrush natural silicon minerals to a particle size of less than 50 micrometers to enhance their reactivity. Under the protection of an inert atmosphere, mineral silicon reacts with active metals (Mg, Al, Zn, etc.)^[84,85] at high temperatures. Upon completion of the reaction, the product undergoes crushing and is sequentially treated with hydrochloric acid and hydrofluoric acid for impurity removal. Although the metallothermic reduction process is relatively mature, its high-temperature operating conditions result in substantial energy consumption costs.

Compared to conventional processes, the molten salt method significantly reduces the reduction temperature. The molten salt facilitates thorough contact between reactants, ensuring uniform reaction progression and preventing localized overheating or

uneven reactions. Simultaneously, the molten salt encapsulates nascent silicon particles and restricts their growth, thereby yielding smaller-sized nanosilicon. Wan et al.^[86] employed the molten salt method to synthesize two-dimensional silicon nanosheets from the layered silicate mineral montmorillonite in a single step. Furthermore, the molten salt accelerates ion diffusion, thereby enhancing the reaction rate, and the generated by-products are dissolved in the molten salt, preventing the encapsulation of unreacted SiO_2 , thus improving the yield of nanosilicon.

The metallothermic reduction method, due to its highly exothermic nature, still faces challenges in controllability and uniformity. Therefore, there is an urgent need to develop a scalable, simple, and cost-effective strategy for the preparation of nanostructured silicon. The mechanochemical reduction method, based on localized high temperatures and intense mechanical forces generated by high-energy mechanical ball milling (such as planetary ball milling), directly initiates solid phase metallothermic reduction reactions while ensuring uniform mixing reactions. This method eliminates the reliance on continuous high-temperature conditions in traditional methods and represents a promising strategy for nanosilicon preparation. Chen et al.^[63] utilized natural talc powder, a layered silicate, as the raw material to prepare hierarchical porous silicon nanosheets via the mechanochemical reduction method. Benefiting from the unique layered structure and chemical composition of talc, the two-dimensional nanostructure of silicon is stably maintained during the exothermic reaction without the need for additional heat scavengers or templates, overcoming the limitations of traditional mechanical reduction methods in precisely controlling silicon nanomorphology. The drawbacks include the susceptibility of product purity to raw material impurities and the need for optimization in energy consumption and efficiency for large-scale production.

3.3. Recycling Technology of Industrial Waste Silicon

Industrial waste silicon primarily originates from cutting waste in the photovoltaic industry, silicon wafer scraps in the semiconductor industry, and by-products of metallurgical silicon processes (silicon sludge and silicon alloy slag). These waste materials typically contain high-purity silicon (>90%) but mostly exist in the form of microsized particles or chunks. The primary methods for preparing nanosilicon from industrial waste silicon include ball milling, molten salt method, metallothermic reduction, carbothermal shock, and metal-assisted chemical etching.

The ball milling method involves the use of high-energy mechanical forces to crush, cold-weld, and repeatedly fracture industrial waste silicon, thereby obtaining nanosized silicon particles.^[87] Its advantages lie in its simple process, absence of high-temperature requirements, and ease of scaling up. However, this method is associated with high energy consumption, potential contamination of the product by milling media, and particle agglomeration due to prolonged grinding.

The metallothermic reduction method can process waste silicon sludge containing SiO_2 , such as photovoltaic head and tail

materials, and silicon alloy waste slag. However, if the content of metal impurities such as Fe and Ca in the waste silicon exceeds 5%, it will affect the product purity, necessitating enhanced purification steps. Wang et al. prepared nanoporous silicon materials from silicon sludge waste using the magnesium thermal reduction method.^[88] Research has shown that the heating rate significantly influences the specific surface area and pore volume of porous silicon, and optimizing the heating rate can improve the silicon nanostructure.

The molten salt method, with its advantages of low-temperature efficiency, product homogeneity, and strong adaptability to raw materials, has become an ideal choice for the high-value utilization of industrial waste silicon, especially low-grade waste silicon containing SiO_2 impurities. This technology offers three significant advantages: 1) simultaneous dissolution and removal of metal impurities such as Fe and Al; 2) direct acquisition of 50–200 nm silicon particles; and 3) production of high-purity silicon materials.

The carbothermal shock method involves mixing waste silicon with a carbon source (such as graphite) and applying ultra-high current or energy in an extremely short time (millisecond level) to achieve ultra-rapid heating ($>1000\text{ }^\circ\text{C min}^{-1}$) and subsequent quenching, thereby realizing nanoscale processing of silicon. The principle lies in the ultra-fast heating rate, inhibiting crystal growth, thus optimizing product morphology (such as nanowires and nanoparticles) through precise control of temperature gradients and reaction time. Shen et al. prepared amorphous silicon nanowires from photovoltaic cutting waste using the carbothermal shock method, utilizing high-temperature gradient fields to drive the directional diffusion of Si atoms in the confined oxidation domain environment of photovoltaic waste.^[71] This method has an extremely short reaction time, relatively low energy consumption, and a small product particle size, but requires high-performance equipment and is currently limited to laboratory scale, posing challenges for industrial scale-up.

The metal-assisted chemical etching method is a preparation technique that utilizes metal catalysts to induce selective etching of the silicon surface. First, the oxide layer on the surface of industrial waste silicon is removed using an HF solution, followed by the deposition of nanoscale metal particles such as Ag, Au, or Pt as catalysts on the silicon surface. The sample is then etched in an $\text{HF}/\text{H}_2\text{O}_2$ mixed solution, where the silicon catalyzed by the metal particles is selectively dissolved, forming porous or nanowire structures. Finally, the metal catalyst is removed using a nitric acid solution to obtain nanosilicon. Zhang et al. prepared silicon nanoparticles from photovoltaic silicon waste using the nanocopper-assisted chemical etching method.^[89] This method allows precise control of the morphology of nanosilicon structures, and the prepared materials have a high specific surface area, but the use of precious metal catalysts results in higher costs, making it suitable for the preparation of nanosilicon with special morphologies.

In summary, developing more cost-effective strategies for the preparation of nanostructured silicon to meet industrial demands is crucial. The methods provide different technical pathways for

nanosilicon preparation, each with its advantages and challenges. Their development and optimization will contribute to advancing related fields. **Table 2** systematically presents the methods for preparing nano-silicon from various silicon sources, along with their respective advantages, disadvantages, and directions for performance optimization.

4. Modification Strategy for Silicon-Based Anode Materials

Recent research has demonstrated the significant promise of low-cost silicon sources as sustainable alternatives to conventional high-purity nanosilicon for lithium-ion battery anodes. These materials offer compelling advantages beyond cost-effectiveness, featuring unique structural characteristics that help address fundamental challenges in silicon anode technology. To fully realize their potential, researchers have developed sophisticated material engineering approaches combining carbon integration, atomic-level doping, and nanostructural design. These advanced modification techniques effectively enhance the electrochemical performance of silicon-based anodes by improving conductivity, accommodating volume changes, and stabilizing interface reactions. This integrated approach to material development not only advances the scientific understanding of silicon anode systems but also provides practical pathways for implementing sustainable battery technologies at an industrial scale.

4.1. Performance Optimization of Biomass Silicon-Based Anode

Biomass-derived silicon, as a sustainable anode material for lithium-ion batteries, offers significant cost advantages through its sourcing from agricultural byproducts like rice husks and straws, enabling high-value utilization of waste resources. Notably, its intrinsic natural porous architecture and hybrid organic-inorganic composition provide an ideal template for constructing nanostructures with inherent volume buffering capabilities. However, practical implementation faces critical challenges: specifically, residual metallic impurities (notably alkali/alkaline earth metals such as K and Ca) compromise electrochemical stability; moreover, the material undergoes substantial volume change during cycling, causing electrode pulverization and accelerated capacity fade; additionally, inherent low electronic conductivity severely restricts rate performance. These limitations collectively constitute significant barriers to commercial deployment despite the material's ecological and economic merits.

To address the multifaceted challenges of biomass-derived silicon anodes, including impurity sensitivity, severe volume expansion, and inherent low conductivity, researchers have developed integrated modification strategies centered on carbon compositing, atomic doping, and structural engineering. Carbon compositing, particularly through *in situ* carbonization leveraging biomass's intrinsic carbon sources, simultaneously enhances

Table 2. A comprehensive summary of the preparation methods utilizing diverse silicon-containing sources.

Classification	Preparation	Advantages	Disadvantages	Performance and optimization	References
Biomass silicon	Hydrothermal method	Mild reaction conditions. Controllable morphology.	Long reaction time. Low yield.	Volume expansion; Optimization of postsynthesis drying to avoid agglomeration.	[81]
	Metallothermic reduction	High yield. Industrial production.	High temperature. Acid waste generation.	High energy consumption; requires energy recovery systems.	[111]
	Mechanochemical reduction	Simple process. Controllable particle size.	High energy consumption. Potential contamination.	Media recycling challenges; surface passivation to prevent impurity diffusion.	[82]
	Molten salt method	Uniform particle size.	Difficult salt recycling.	High costs; develop salt formulations.	[83]
Mineral silicon	Metallothermic reduction	Suitable for high-purity quartz. High crystallinity.	High energy consumption. Require HF treatment.	Impurity segregation; <i>in situ</i> purification to meet battery-grade standards.	[84,85]
	Mechanochemical reduction	No sustained high temperature. Relatively low energy consumption.	Impurities affect purity. Difficult morphology control.	Phase separation; surface modification strategies and structural design.	[63]
Industrial waste silicon	Molten salt method	Processes low-grade ores, efficient impurity removal.	Potential salt residue. High equipment corrosion.	Limited scalability for ultrafine particles; optimize the ion dispersion strategy.	[86]
	Ball milling	Easy scaling. No high temperature.	Risk of contamination.	Long milling times; inhibit aggregation.	[87]
	Molten salt method	Easily remove impurities. High purity.	Complex equipment. Short lifespan.	Electrode erosion; coating modification.	[119]
	Carbon thermal shock	Ultrafast reaction. Small particles.	High equipment requirements. Limited to lab scale.	Brittle carbon-silicon interface; carbon coating and interfacial design strategies.	[71]
	Metallothermic reduction	Process SiO ₂ -containing waste. Heating rate controls porosity.	Require intensive purification. Exothermic reaction control.	The porosity of particles; optimize the heating rate, time, and temperature.	[88]
	Metal-assisted chemical etching	Precise morphology control. High specific surface area.	Noble metal catalysts. High cost.	High fabricating costs; recycle the catalyst to reduce costs.	[89]

electronic conductivity while creating a conformal buffer layer that mitigates mechanical stress during lithiation.^[90,91] Complementarily, atomic doping with elements such as nitrogen, phosphorus, or sulfur modulates the electronic structure at the atomic scale, optimizing charge distribution and strengthening interfacial bonds to stabilize the SEI, thereby accelerating lithium-ion diffusion kinetics.^[92] Further performance gains are achieved through deliberate structural design: engineered architectures including interconnected porous networks accommodating particle expansion without fracture, vertically aligned nanowires shortening ion diffusion paths while withstanding radial strain, and core–shell configurations spatially confining volume changes within carbon-encapsulated domains.^[93]

Si/C composites synergistically integrate the exceptional theoretical capacity of silicon with the structural resilience and conductivity of carbon, thereby significantly enhancing the comprehensive electrochemical performance of lithium-ion battery anodes. Based on carbon source incorporation methodologies, these composites are classified into two primary categories: *in situ* carbon composites and external carbon composites. Biomass-derived silicon sources leverage their intrinsic advantages by containing 15–20 wt% organic components. Through controlled carbonization under an inert atmosphere, these organic constituents are directly converted into three-dimensional conductive carbon networks that encapsulate silicon particles. As shown in Figure 5a, Aini et al.^[94] utilized wild herbaceous plants to prepare SiO_x/C composites. During the annealing of the dense SiO₂ matrix of the goosegrass leaves, the uniformly distributed organic carbon inside was not oxidized and decomposed but formed an *in situ* carbon network, which was tightly bonded with SiO_x (Figure 5c). This dense SiO_x matrix, combined with the uniformly dispersed carbon structure, brings higher active SiO_x content, larger specific surface area, and abundant carbon defect sites, thereby significantly improving the material's specific capacity, cycling stability, and rate performance. Specifically, the SiO_x/C anode maintains a charge/discharge specific capacity of 704 mAh g⁻¹ after 500 cycles and realizes a charge/discharge specific capacity of 330 mAh g⁻¹ at a high current density of 1 A g⁻¹ (Figure 5b).

Although the *in situ* carbonization of the inherent carbon source in biomass offers advantages like low cost and a simple process, the pore distribution, specific surface area, and micro-morphology of biomass-derived carbon are significantly influenced by the type of feedstock and pyrolysis conditions. This leads to poor batch-to-batch consistency. Conversely, external carbon sources (such as graphite, carbon nanotubes, and carbon derived from organic precursors) possess the advantages of homogeneous morphology and a tunable pore structure (mesopore/microporous), enabling more precise optimization of the ion/electron transport path of the electrodes. As shown in Figure 5d, Guo et al.^[95] prepared composites with SiO_x nanoparticles uniformly dispersed in a spherical nitrogen-doped carbon matrix by the electrospray-carbonization method using rice husk as a silicon source. The carbon framework effectively inhibits the aggregation of SiO_x particles, promotes ion diffusion and charge transfer, and maintains structural stability during cycling. As an

anode material, the SiO_x/NC electrode exhibits a stable specific capacity of 622.8 mAh g⁻¹ after 100 cycles at a current density of 0.1 A g⁻¹, and at a high current density of 5 A g⁻¹ after 5000 cycles, it still maintains a specific capacity of 190.1 mAh g⁻¹ charge/discharge specific capacity (Figure 5e). *In situ* XRD analysis during cycling revealed that the formation of a stable SEI film significantly enhances the cycling stability of the anode (Figure 5f). Also, as exhibited in Figure 5g, Zhang et al.^[55] employed an electrospray method to prepare a SNCC nano/microstructured spheres composite. SEM image shows that the Si NPs are uniformly encapsulated in the N-doped carbon matrix with inserted CNTs (Figure 5h). The structure promotes rapid electron transfer, effectively prevents silicon pulverization, and maintains good structural stability. Thereby, the SNCC spheres electrode exhibits an excellent rate performance, at the current density of 0.1 and 1 A g⁻¹, the SNCC spheres electrode achieves a specific capacity of 1460 and 978 mAh g⁻¹, respectively, corresponding to a capacity retention of 67% at high rate (Figure 5i).

Atomic doping can modulate the electronic structure and surface chemistry of biomass silicon, which is an effective strategy to enhance the properties of silicon–carbon composites. As shown in Figure 6a, Guo et al.^[96] proposed a pervasive electrospray-carbonization method for preparing ternary metal (Fe, Co, Ni)/SiO_x/nitrogen-doped carbon composite structures to enhance the long-cycle-life performance of lithium-ion battery anodes. The introduced metal nanoparticles (especially the ultra-small-sized Ni nanoparticles) can significantly improve the overall electrical conductivity of the material and effectively promote electron transport within the material, thus improving the rate capability of the battery. Among them, the Ni/SiO_x/NC composite maintains a reversible discharge specific capacity of 665.0 mAh g⁻¹ after 500 cycles, and 116.3 mAh g⁻¹ after 5000 cycles even at a high current density of 10 A g⁻¹ (Figure 6b). In addition, carbon doping by nonmetallic heteroatoms (e.g., P, N, and B) can effectively improve the conductivity of silicon materials and provide pseudocapacitance and additional lithium-ion storage sites. Meanwhile, the doped atoms can also inhibit the decomposition of the electrolyte to some extent, improving the initial Coulombic efficiency.

Cui et al.^[97] synthesized an N@C/SiO_x composite through a simple pyrolysis process, as shown in Figure 6c. The N@C/SiO_x electrode exhibits a high reversible discharge specific capacity of 1018.5 mAh g⁻¹ at a current density of 0.1 A g⁻¹. Under a test condition of 1.0 A g⁻¹, the capacity decay is only 4.0% after 1000 cycles (Figure 6d). Except for graphite N, the presence of N atoms in the other three chemical states mentioned above can introduce some defects into the C skeleton of N@C/SiO_x samples and thus improve their Li⁺ storage capacity (Figure 6e). N-doping improves the electronic conductivity of the carbon skeleton and alleviates the volume expansion of the SiO_x. The porous structure facilitates electrolyte wetting and Li⁺ transport. Moreover, nitrogen atoms provide additional lithium storage sites and pseudocapacitance contributions, and inhibit part of the electrolyte decomposition, thereby improving the initial Coulombic efficiency (72.2%).

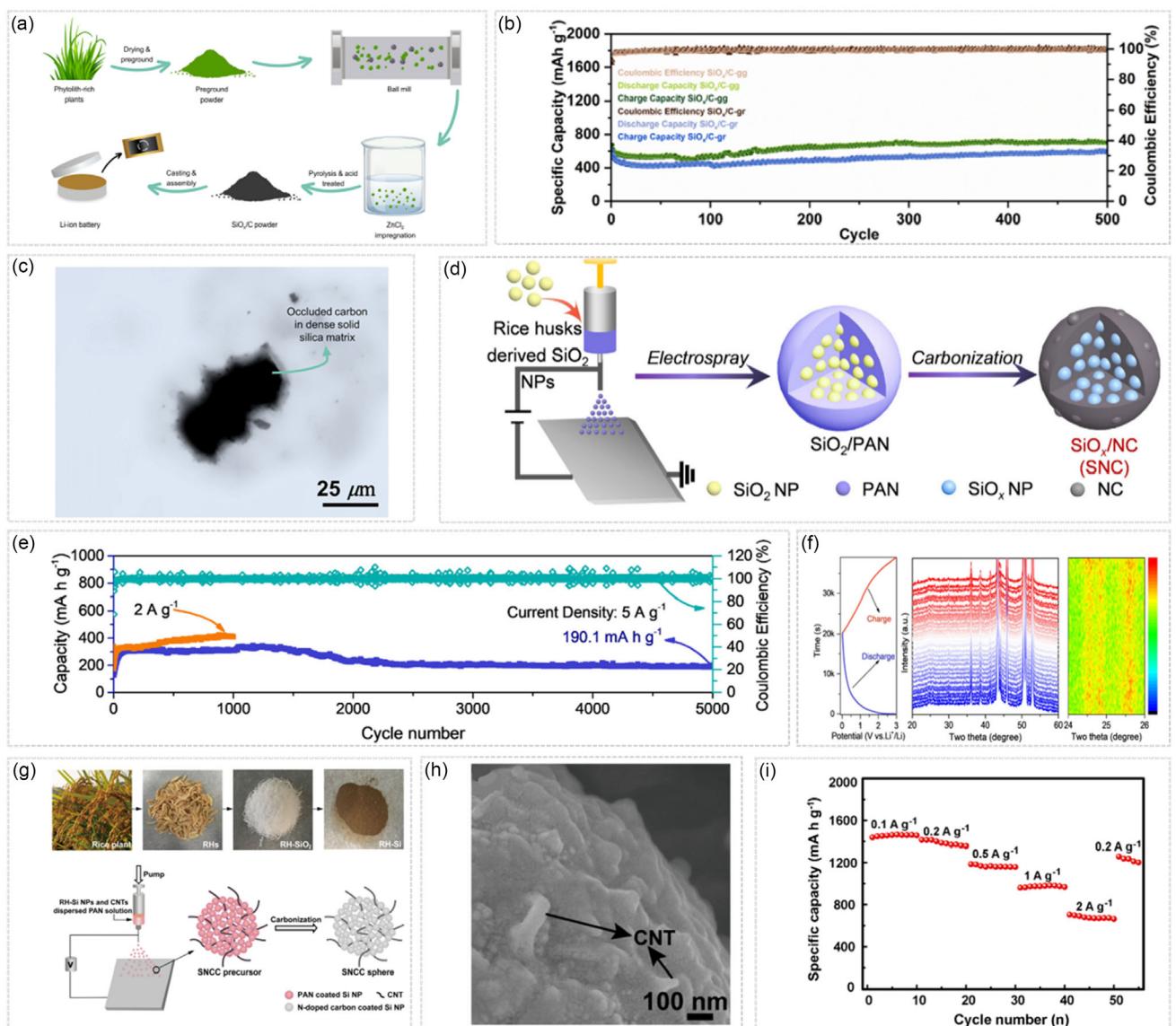


Figure 5. a) Schematic synthesis procedure for SiO_x/C derived from phytolith-rich plants for lithium-ion battery anode applications. b) Cycling performance and Coulombic efficiency comparison of different SiO_x/C anodes at 200 mA g^{-1} . c) Transmission electron microscope (TEM) image of the SiO_x/C . Reproduced with permission.^[94] Copyright 2024, American Chemical Society. d) Schematic synthesis of a series of SiO_x/N -doped carbon (SNC) microspheres. e) Long cyclability of SNC-2 (containing 0.125 g SiO_2 NPs) at 2 A g^{-1} and 5 A g^{-1} . f) The charge/discharge curve and corresponding in situ X-ray diffraction (XRD) patterns of the SNC-2 electrode and the corresponding high-resolution contour maps. Reproduced with permission.^[95] Copyright 2021, Elsevier. g) Schematic illustration of the preparation process for silicon/nitrogen-doped carbon/carbon nanotube (SNCC) nano/microstructured spheres. h) High magnification Scanning electron microscope (SEM) image. i) Rate performance of the SNCC spheres electrode at various currents. Reproduced with permission.^[55] Copyright 2016, Elsevier.

Biomass silicon has a unique natural porous structure, and its electrochemical properties can be significantly enhanced through rational structurization design. The structuring of biomass silicon mainly includes two major directions: natural structure utilization and artificial structure modulation. As shown in Figure 6f, Chen et al.^[98] transformed bamboo shoot shells into hierarchical porous SiO_x/C materials through low-temperature activation and aluminum thermal reduction, preserving the original tubular structure. This structure forms a stable porous carbon framework that supports the uniform distribution of SiO_x particles. As a result, the hierarchically porous SiO_x/C composite

anode exhibits an initial discharge specific capacity of 1332 mAh g^{-1} at a current density of 200 mA g^{-1} and maintains a capacity of 1289 mAh g^{-1} after 400 cycles (Figure 6g), with a high Coulombic efficiency of 94.41%. The volume expansion rate is reduced to 44.7%, significantly lower than that of traditional silicon-based materials. In addition to utilizing its porous structure, the preparation of silicon into nanowire structures with a high specific surface area for use as a lithium-ion anode can provide more active sites for lithiation/delithiation. As shown in Figure 6h, Pang et al.^[99] proposed a sustainable molten salt leaching-electrodeposition method for the conversion of rice husk

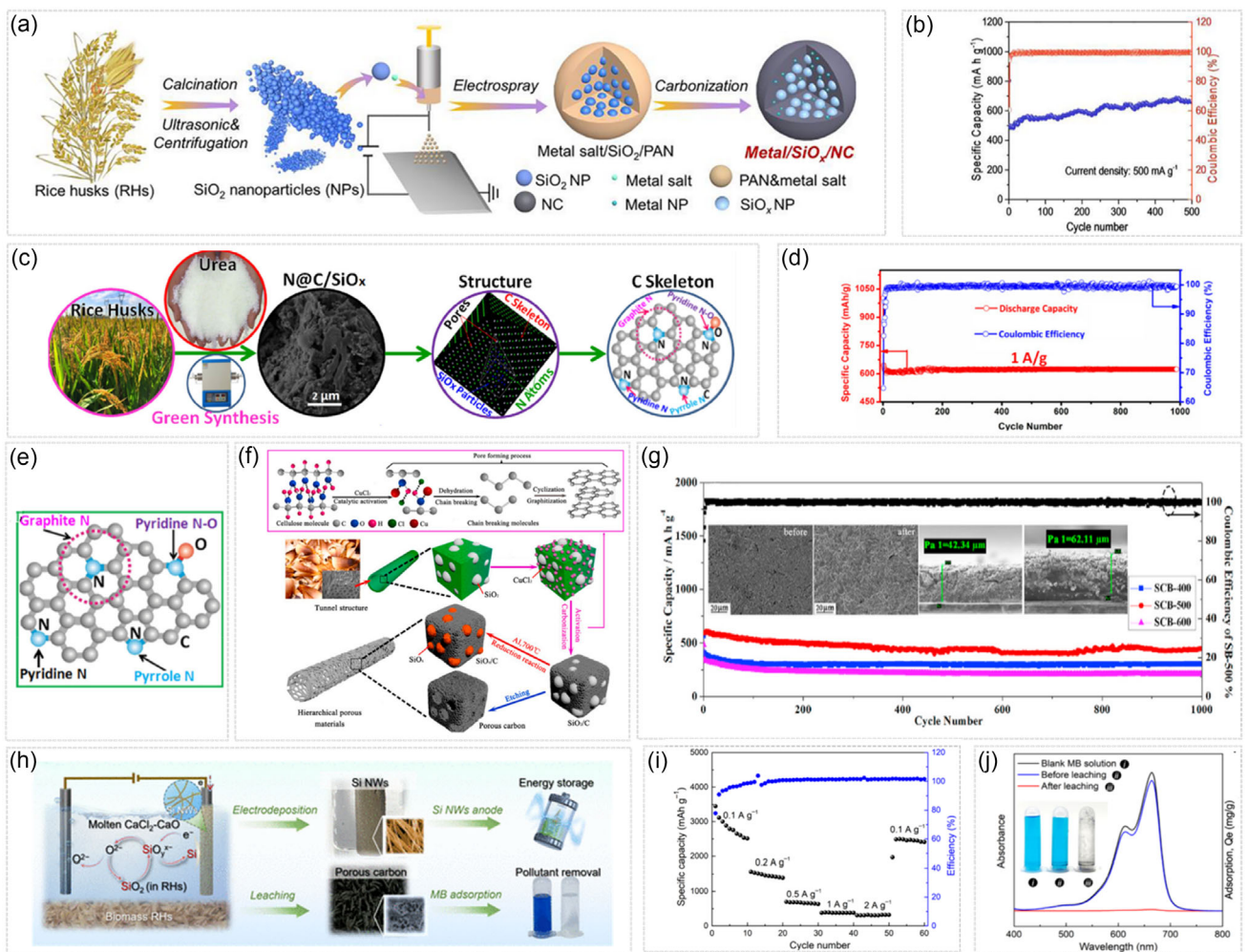


Figure 6. a) Schematic synthesis of metal/SiO_x/NC superstructures. b) Long cyclability of the Ni/SiO_x/NC at 500 mA g⁻¹. Reproduced with permission.^[96] Copyright 2021, Elsevier. c) Green synthesis of N-doped carbon-coated SiO_x (N@C/SiO_x) composite. d) Long-term cycling stability at 1.0 A g⁻¹ for 1000 cycles of N@C/SiO_x electrode. e) Illustration of N-doped C skeleton with different doping sites. Reproduced with permission.^[97] Copyright 2020, Elsevier. f) Schematic of the overall synthetic process of the SiO_x/C and porous carbon from bamboo shoot hulls at 400–600 °C at the current density of 3000 mA g⁻¹ (inset: SEM images of the SCB-500 electrode before and after cycling). Reproduced with permission.^[98] Copyright 2021, Elsevier. h) Schematic illustration of the sustainable conversion of RHs into Si nanowires and porous carbon. i) Capacities and coulombic efficiency at the current density range of 0.1–2 A g⁻¹. j) UV-vis adsorption spectra and optical images of methylene blue (MB) solution (20 mg L⁻¹) adsorbed by carbonized RH powder before and after leaching in molten salt. Reproduced with permission.^[99] Copyright 2024, American Chemical Society.

biomass into functional silicon nanowires and porous carbon materials, followed by the direct extraction of silicon nanowires by controlled electrodeposition. The formation of silicon nanowires is achieved by electrochemical reduction of silicate ions, and the growth mechanism is influenced by the surface energy, with silicon tending to grow along the^[100] direction to form nanowire structures with high aspect ratios. This structural modification not only improves the crystallinity of the silicon nanowires but also significantly enhances their cycling stability in the battery by forming an amorphous SiO₂ shell layer on the surface. The Si nanowire anode delivers a high first discharge capacity of 3447.8 mAh g⁻¹ and a subsequent discharge capacity of 2514 mAh g⁻¹ at 0.1 A g⁻¹ after 10 cycles (Figure 6i). Particularly, the RH-derived porous carbon materials can also be directly used for organic adsorption applications with

99.1% adsorptive removal of methylene blue (50 mg) per gram of porous carbon (Figure 6j). Also, Li et al.^[101] prepared C/SiO₂ composites with a core-shell structure from rice husk using a combined alkali extraction and acid precipitation method. The carbon shell layer not only acts as an efficient conductive network but also effectively buffers the volume change, thus improving the cycling stability and lifetime of the material. As a result, the reversible discharge specific capacity is maintained at 534 mAh g⁻¹ even after 1000 cycles at a current density of 1 A g⁻¹.

4.2. Reinforcement Pathways of Mineral Silicon-Based Anodes

Mineral silicon, sourced from quartzite, diatomaceous earth, and analogous geological deposits, represents a strategically vital

precursor for silicon-based anodes, offering compelling advantages including abundant natural reserves, low extraction costs, and scalable availability that support mass production. However, practical implementation confronts persistent challenges: significant volume expansion, inducing electrode degradation, and intrinsically poor electrical conductivity, impairing rate capability.^[102] To address these dual limitations, integrated modification strategies prove essential: conformal carbon coating enhances electronic conductivity while buffering mechanical stress, targeted elemental doping (e.g., N, P) optimizes charge transfer kinetics and interfacial stability, and deliberate structural engineering (porous architectures, yolk-shell configurations) accommodates volumetric strain.^[103] Synergistically applied, these approaches transform mineral silicon's inherent advantages into functional anode performance, overcoming application bottlenecks and enabling next-generation high-capacity lithium-ion batteries through economically viable, resource-sustainable pathways.

As illustrated in Figure 7a, Zhu et al.^[104] successfully synthesized carbon-coated silicon nanosheet composites using a one-pot strategy with natural talc as the silicon source. First, talc was mixed with magnesium powder for magnesium thermal reduction, followed by carbon deposition using CO₂ as the carbon precursor. Although the XRD pattern did not show distinct signals from the amorphous carbon coating due to its ultrathin nature and low content, the high-resolution transmission electron microscopy (HRTEM) image of the Si/C composite revealed a uniform 3 nm amorphous carbon layer surrounding the well-crystallized Si particles (Figures 7b,c). Besides, as shown in Figure 7d, X-ray photoelectron spectroscopy (XPS) survey spectra confirmed the presence of carbon on the surface of the Si/C composite, unambiguously demonstrating the successful synthesis of the Si/C composite material. The prepared Si/C composite, consisting of carbon-coated silicon nanosheets, exhibits excellent electrochemical performance as a lithium-ion battery anode. Similarly, Bao et al.^[105] proposed the simultaneous synthesis of porous

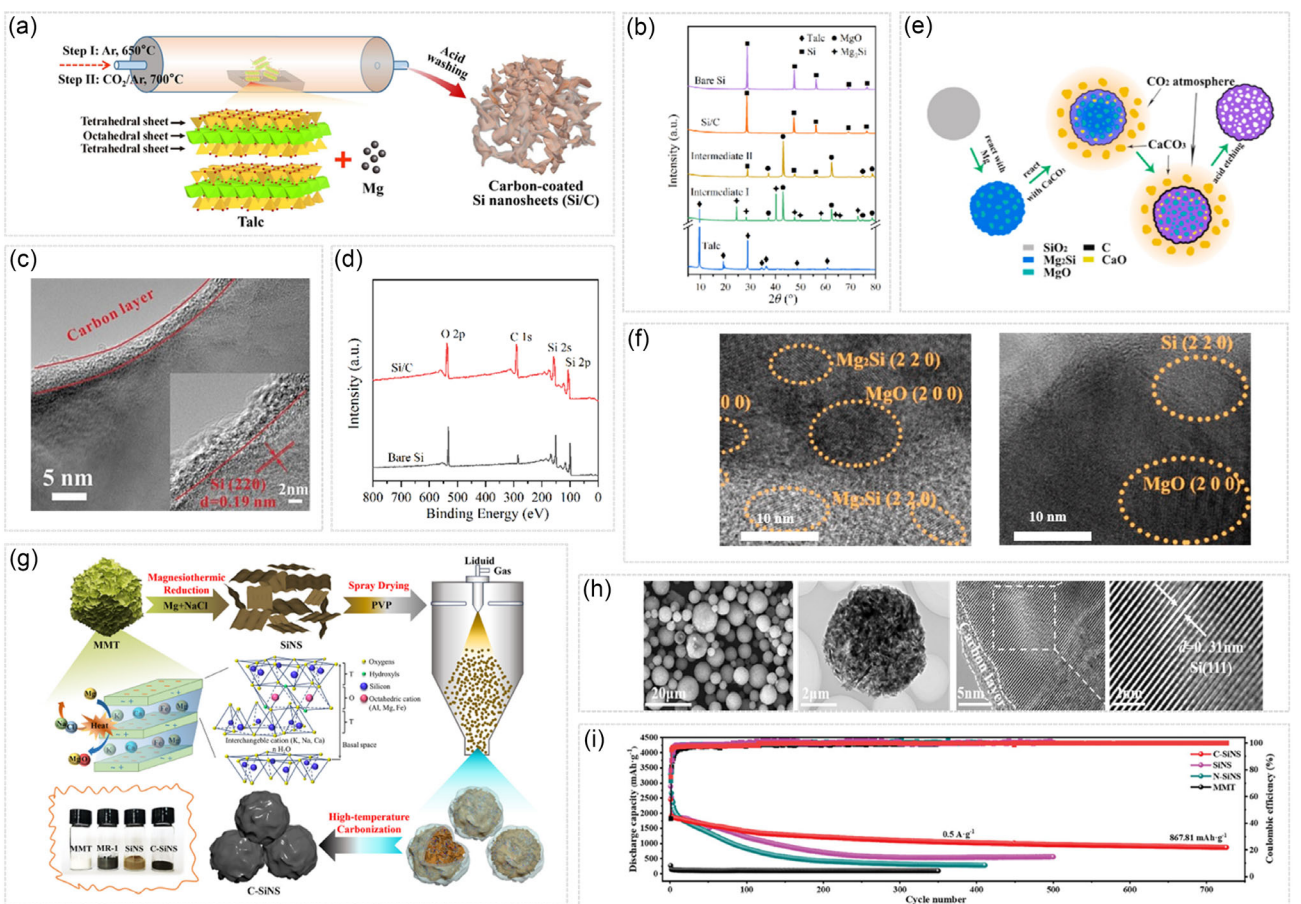


Figure 7. a) Schematic illustration of the one-pot synthesis of the carbon-coated porous silicon nanosheets (Si/C). b) XRD patterns of purified talc, the intermediate I after magnesiothermic reduction reaction, the intermediate II after reaction with CO₂, the corresponding product Si/C, and the product bare Si after the removal of carbon coating. c) HRTEM image of the insect showing crystalline structure. d) XPS survey spectra of bare Si and Si/C. Reproduced with permission.^[104] Copyright 2024, Elsevier. e) Schematic illustration of the reaction from the SiO₂ sphere to the final Si@C composite. f) HRTEM images of the as-prepared Mg₂Si spheres reacted with CaCO₃ after different reaction times: 0 and 5 h, respectively. Reproduced with permission.^[105] Copyright 2021, Elsevier. g) Schematic of the synthesis for carbon-coated silicon nanosheets (C-SiNS). h) SEM image and TEM image of C-SiNS, and HRTEM images of C-SiNS at different magnifications (pyrolytic carbon, lattice fringes of Si), and i) long-cycle performance of C-SiNS at 0.5 A g⁻¹. Reproduced with permission.^[86] Copyright 2025, Wiley.

Si@C composites as shown in Figures 7e,f. Using diatomite as the raw material, SiO_2 spheres were obtained as the silicon precursor, which was then converted to Mg_2Si spheres via a magnesium reduction reaction. Subsequently, carbon nanolayers were formed by reacting with calcium carbonate. Figure 7f exhibits HRTEM images of the as-prepared Mg_2Si spheres reacting with CaCO_3 after different reaction times. After 5 h of reaction, all Mg_2Si was converted to Si. The resulting porous Si@C composite material, containing carbon nanolayers, effectively alleviates the volume expansion during silicon lithiation, enhances electrical conductivity and structural stability, and significantly improves electrochemical performance. Ma et al.^[86] proposed the preparation of Si/C composites by using organic polymers as carbon precursors, as shown in Figure 7g. Two-dimensional SiNS were first prepared from montmorillonite by the molten salt-assisted magnesium thermal reduction method, and the SiNS were mixed with polyvinylpyrrolidone (PVP), which was spray pelletized and pyrolyzed at high temperature, to obtain high-sphericity Si/C composites. As shown in Figures 7h,i, the microstructure diagram of C-SiNS reveals its morphology and elemental composition, forming a uniform amorphous carbon layer on the surface of silicon. These materials exhibit excellent cycling stability. Doping with other atoms can also improve the electrical conductivity of silicon-based anode materials. Ding et al.^[112] produced $\text{SiO}_2@\text{Al}$ composites by combining SiO_2 from natural porous structured diatomite with aluminum foil ball-milled by a melt self-assembly method and then reacted at high temperatures in a tube furnace to infuse molten aluminum atoms into the diatomite. Figure 8a,b presents the SEM image of the material, and some pores can still be seen on the surface of the diatomite. The prepared $\text{SiO}_2@\text{Al}$ electrode maintains a capacity of 735 mAh g⁻¹ after 300 cycles with a capacity retention rate of 95% (Figure 8c). Moreover, the structural design of silicon-based anode materials is an important means to alleviate volume expansion, and the special structure of natural minerals offers significant advantages in this regard. Chen and his co-authors^[113] prepared micrometer-sized layered silicon with high vibrational density (0.9–1.0 g cm⁻³) from montmorillonite, an economical, naturally occurring layered silicate mineral, using a localized reduction technique, as shown in Figure 8d. The mesoporous structure within each layer synergizes with the interlayer voids to effectively mitigate the lateral and vertical expansion in the lithiation/delithiation cycle, and the residual SiO_2 network strengthens the lamellar structure to prevent collapse in the cycle. Besides, Zhao et al.^[85] obtained three-dimensional porous silicon flakes by chemical reduction of layered talc clay minerals containing metal oxides (Figure 8e).

This clay mineral consists of two layers of silica-oxygen tetrahedra sandwiched by a single layer of magnesium oxide and hydroxide, and the metal oxide layer serves as a negative catalyst during the reduction reaction, absorbing the heat released from the reaction between the silicate layer and the metal reducing agent, slowing down the rate of the reaction, and preventing structural damage. Therefore, the obtained anode with an excellent rate capability and stable Coulombic efficiency (Figure 8f). Recently, Li et al.^[106] reported a scalable approach: the electrochemical reduction of attapulgite in molten salt and the

preparation of stacked silicon nanosheets through acid washing, as depicted in Figures 8g-i. Comprising three-dimensional stacked silicon nanosheets and numerous voids, this material can accommodate the volume expansion that occurs during lithiation/delithiation. Benefiting from this, the thickness of the s-SiNS coating layer changed from 7 to 11 μm , with an expansion rate of 57.1%, and the stacked silicon nanosheet anode provides a high specific capacity of up to 3046 mAh g⁻¹ and a high initial Coulombic efficiency of 82.5% under 0.2 A g⁻¹.

4.3. Regulation Methods of Industrial Waste Silicon-Based Anodes

Industrial waste silicon (e.g., metallurgical slag) offers sustainable, low-cost anode potential with high purity and crystalline integrity. Implementation barriers include: surface oxide impeding Li⁺ transport; volume expansion causing structural collapse; and intrinsically low Li⁺ diffusion limiting rate capability.^[100,107] Researchers have developed integrated modification strategies: conformal carbon coating enhances conductivity while buffering mechanical stress and suppressing parasitic interfacial reactions; targeted elemental doping (e.g., B, Ag) modulates silicon's electronic structure to improve Li⁺ diffusivity and charge transfer kinetics; and deliberate structural engineering shortens ion diffusion paths while maximizing electrode–electrolyte interface contact area.^[108]

Exemplifying this approach, as shown in Figures 9a,c, Wan et al.^[114] engineered Si/CNTs/C composites from photovoltaic kerf waste through polishing (yielding < 100 nm Si particles), spray-drying with CNTs and PVP, and carbon coating, achieving this via synergistic strain accommodation and conductive networking. The synthesized Si/CNTs/C composite material has a residual capacity of more than 1000 mAh g⁻¹ after 500 cycles at 1 A g⁻¹ current (Figure 9b). Similarly, Ahn et al.^[115] fabricated Si/rGO composites by surfactant-assisted self-assembly of recycled Si nanoparticles with GO, followed by freeze-drying and thermal reduction (Figures 9d,e). The obtained composite exhibits 2300 mAh g⁻¹ initial capacity at 100 mA g⁻¹ and 72% capacity retention after 300 cycles at 200 mA g⁻¹ (Figure 9f), where rGO provides both conductive pathways and volume expansion confinement. Building upon foundational modification strategies, researchers have developed innovative composite architectures to address silicon anode limitations. Lee et al.^[116] engineered graphite-reinforced nanosilicon/asphalt composites through two-step pyrolysis, where thermally activated asphalt derivatives greatly enhanced electronic conductivity while preventing nanoparticle aggregation and mitigating volume fluctuations (Figures 9g,h). Consequently, the pyrolyzed silicon/asphalt exhibits an impressive initial discharge capacity (2197 mAh g⁻¹) and an initial Coulombic efficiency of 75%.

Simultaneously, as exhibited in Figure 10a, Meng et al.^[117] created spherical jackfruit-like silicon–carbon structures embedding crystalline silicon nanoparticles within amorphous carbon matrices; this unique topology reduces electrolyte-exposed surface area while maintaining efficient electron pathways and

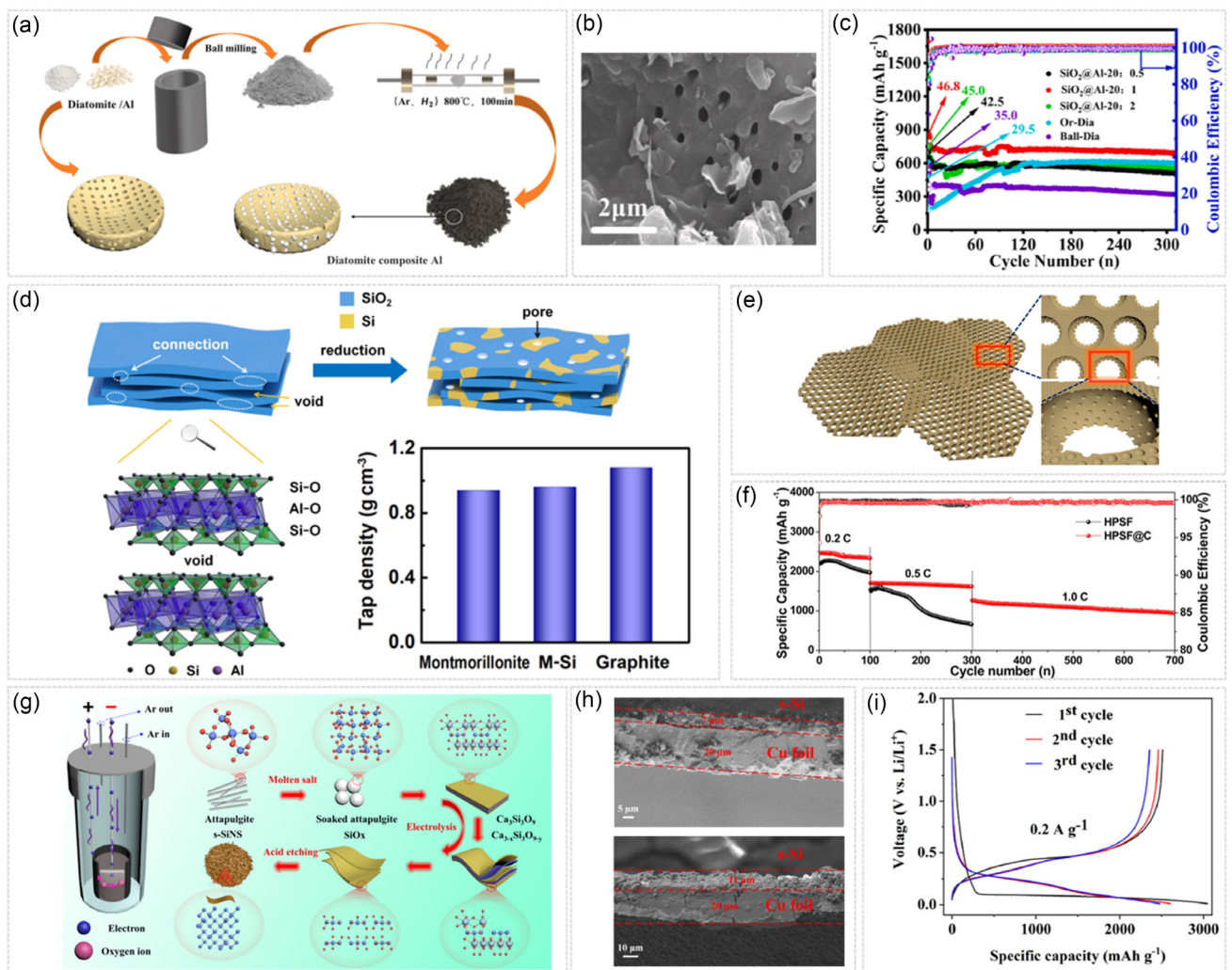


Figure 8. a) Preparation process diagram of electrode material $\text{SiO}_2@\text{Al}$. b) SEM image of $\text{SiO}_2@\text{Al}$ electrode, and c) the cycle performance comparison of varied samples at a current density of 100 mA g^{-1} . Reproduced with permission.^[112] Copyright 2023, Elsevier. d) Illustration of montmorillonite-derived Si (M-Si), and corresponding tap density of the three samples. Reproduced with permission.^[113] Copyright 2024, American Chemical Society. e) Schematic illustration of 3D hyperporous structure flakes (HPSF). f) Long-term cycling stability of HPSF and HPSF@C electrode at a rate of 0.2 C, 0.5 C, and 1.0 C. Reproduced with permission.^[85] Copyright 2016, American Chemical Society. g) The schematic illustration of the general preparation process of s-SiNS. h) Cross-sectional SEM images of the s-SiNS anodes: before and after 100 cycles at 0.5 A g^{-1} , and i) initial three voltage-capacity profiles of the s-SiNS anodes at 0.2 A g^{-1} . Reproduced with permission.^[106] Copyright 2022, Elsevier.

dispersing mechanical stress. Compared with nanosilicon anodes, this composite anode exhibits better cycling performance (Figure 10b). Complementing these carbon-focused approaches, Yin et al.^[118] transformed waste glass precursors via magnesio-thermic reduction into mesoporous silicon particles featuring interconnected 2D nanoplates, a dual-functional architecture that simultaneously accommodates volume changes and facilitates rapid Li^+ diffusion, as illustrated in Figure 10c,d. The prepared mesoporous Si particles exhibit excellent lithium storage performance, exhibiting a high initial capacity of 1793 mAh g^{-1} after 120 cycles at 200 mA g^{-1} .

Further advancing interfacial engineering, Peng et al.^[109] developed N-doped Si/C composites from photovoltaic waste: acid-purified silicon nanosheets were uniformly coated with nitrogen-doped carbon derived from dopamine pyrolysis, where

the carbon matrix buffers expansion while nitrogen doping modulates electronic structure to accelerate Li^+ kinetics (Figure 10e). Compared with pure silicon materials, the morphology of silicon nanosheets protected by nitrogen-doped carbon does not fracture after delithiation, which is also demonstrated by the post-mortem SEM observation (Figure 10f). Similarly, Luo's group constructed P-SiNPs/Ag@C composites using silicon wafer waste through phenolic resin pyrolysis with secondary silver decoration; the synergistic combination of porous architecture, conductive carbon coating, and embedded silver nanoparticles enabled exceptional conductivity and volume change tolerance (Figures 10g,h). As a result, the P-SiNPs/Ag@C anode retains a reversible specific capacity of 1521 mAh g^{-1} after 50 cycles at a current density of 0.2 A g^{-1} ^[110]. These case studies collectively demonstrate how strategic material design transforms diverse

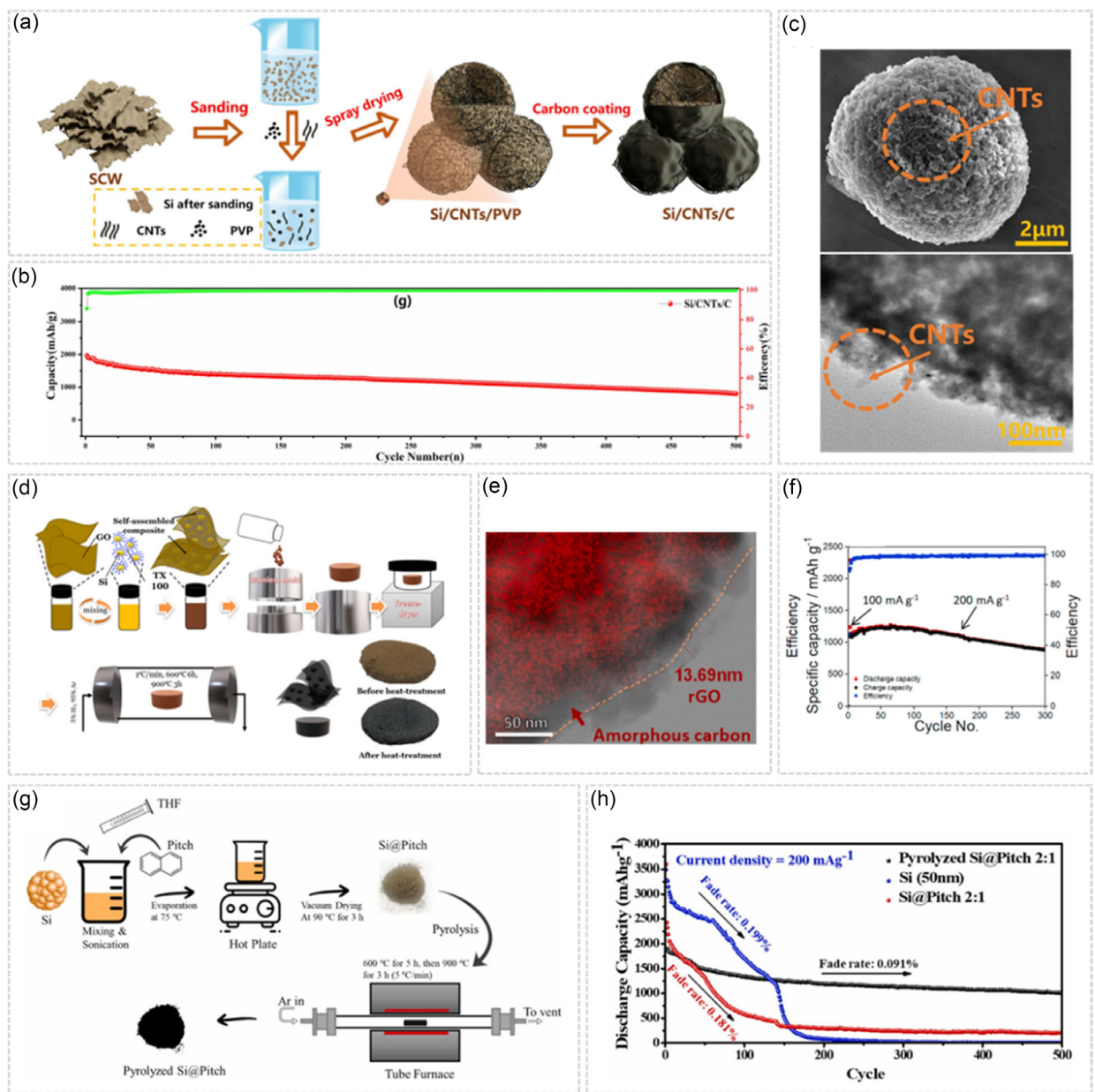


Figure 9. a) Schematic diagram of the synthesis of Si/CNTs/C. b) Long-term cycling performance of Si/CNTs/C composite at 1 A g⁻¹. c) SEM image and TEM image of Si/CNTs/C. Reproduced with permission.^[114] Copyright 2023, Elsevier. d) Schematic of self-assembled composite preparation assisted by Triton X-100. e) Overlayed energy dispersive X-ray detector element mapping area of Si, and f) Long cycle-life test at a current density of 200 mA g⁻¹. Reproduced with permission.^[115] Copyright 2021, Elsevier. g) Illustration of the Si@Pitch synthesis process. h) Cycling performances of pyrolyzed Si@Pitch-2:1, Si(50 nm), and Si@Pitch-2:1 anodes at a current density of 200 mA g⁻¹. Reproduced with permission.^[116] Copyright 2023, Elsevier.

silicon sources into high-performance anodes. As a precursor for high-performance silicon–carbon composite anodes, low-cost silicon sources exhibit remarkable advantages in lithium-ion batteries. However, its practical implementation is still hindered by issues such as impurity management, significant volume expansion, and insufficient conductivity. To comprehensively address these limitations, future endeavors should incorporate synergistic modification strategies. For instance, atomic doping can be combined with structural engineering, or heteroatom incorporation can be paired with external carbon compositing. Such combinatorial methods allow for the co-optimization of

crucial performance parameters. Specifically, they can achieve a high specific capacity (greater than 1500 mAh g⁻¹) by maximizing silicon utilization, enhancing rate capability through the improvement of electronic/ionic conductivity, extending the cycle life beyond 1000 cycles by stabilizing the electrode architecture, and limiting volume change to less than 50% via hierarchical buffering. This integrated innovation paradigm will establish a robust material foundation for next-generation high-energy-density lithium-ion batteries while advancing the sustainable valorization of silicon-containing resources.

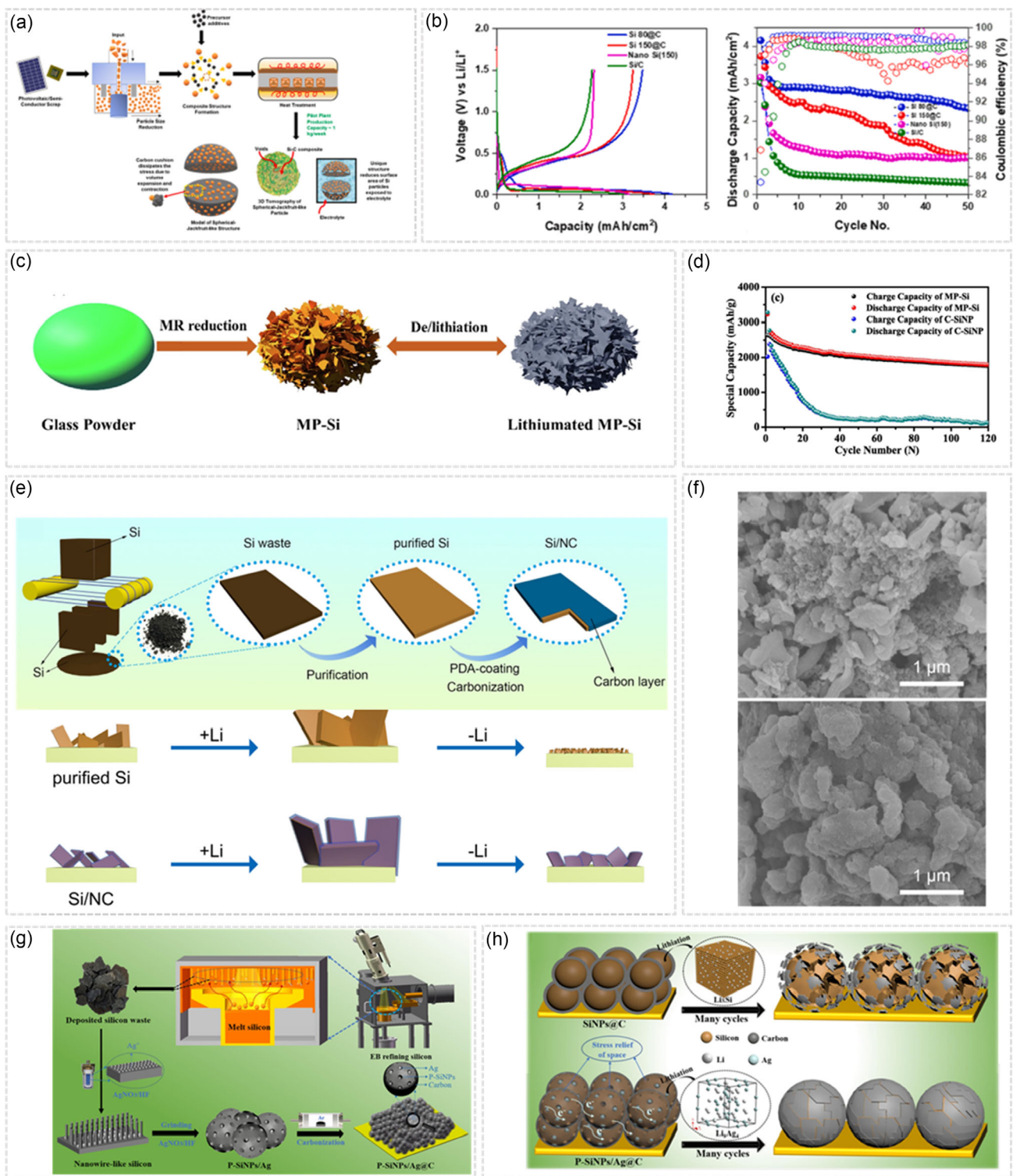


Figure 10. a) Schematic describing the recycling process chain of Si scrap. b) Charge-discharge profile of nano Si (150), Si/C, Si 150@C, and Si 80@C (the number specifies the nominal particle size of the silicon powder) cells and following cycle performance. Reproduced with permission.^[117] Copyright 2023, Elsevier. c) Synthetic process of the MP-Si anode. d) The cycling performance of MP-Si and C-SiNP. Reproduced with permission.^[118] Copyright 2019, Elsevier. e) Schematic illustration of the Si/NC. f) SEM images of anodes after 50 cycles. Reproduced with permission.^[109] Copyright 2021, Elsevier. g) The illustration of porous silicon/silver@carbon (P-SiNPs/Ag@C) synthetic procedure; h) the main failure schematic diagram of SiNPs@C and P-SiNPs/Ag@C structure during lithiation/delithiation. Reproduced with permission.^[110] Copyright 2022, Elsevier.

The distinct physicochemical signature of each silicon source governs the primary consideration for its modification strategy. Biomass silicon, with its inherent hierarchical porosity and organic carbon, is uniquely suited for *in situ* carbonization and hetero-atom doping, leveraging its natural structure to simultaneously address conductivity and volume change. In contrast, mineral silicon sources, such as layered silicates or diatomite, offer predefined morphological templates that direct the synthesis towards structurally engineered composites like 2D Si/C, often augmented by metallothermic reduction and elemental doping to enhance interfacial stability. Industrial waste silicon, despite its high purity, presents variable metallic impurities and surface oxides, mandating rigorous prepurification followed by precisely controlled conductive coating or catalytic doping to mitigate performance fluctuations and ensure batch-to-batch consistency.

5. Conclusion and Perspective

5.1. Summary

Silicon-based anodes, pivotal for next-generation high-energy-density batteries, require sustainability and performance optimization. This work systematically assesses three low-cost silicon sources, biomass-derived, mineral, and industrial waste, demonstrating that strategic source selection and process refinement enable high electrochemical performance and cost efficiency. Biomass leverages intrinsic porosity; mineral sources facilitate scalable production via nanostructuring; waste silicon promotes resource circularity. Core challenges of inadequate integrated carbon compositing, atomic doping, and structural engineering. Persistent industrial barriers remain: biomass faces seasonal supply volatility; mineral processing conflicts with decarbonization imperatives; waste silicon exhibits heterogeneous impurities limiting purification scalability.

5.2. Future Perspective

5.2.1. Strategic Silicon Source Development

As illustrated in Figure 11, the evolution of silicon sources must prioritize novel solutions, balancing purity, cost, and sustainability. Biomass silicon's environmental merits, natural porosity, and organic-inorganic hybrid frameworks are counterbalanced by seasonal supply volatility and low silicon yield, restricting scalability. Mineral silicon offers geological abundance and compositional stability, but suffers from energy-intensive traditional metallurgy incompatible with decarbonization targets. Industrial waste silicon delivers high baseline purity and mature collection systems, yet variable impurity profiles (contaminants like Fe/Al) necessitate source-specific purification protocols. Next-generation sources should integrate closed-loop material flows, leveraging computational screening to identify underutilized silica-rich streams (e.g., phytolith-rich crops, low-grade

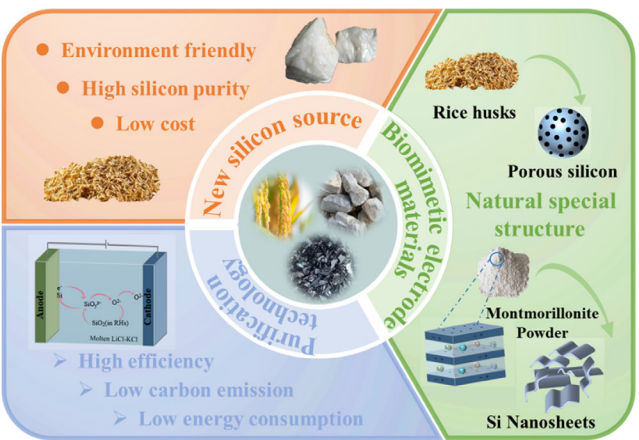


Figure 11. Outlook on silicon-based anode materials from silicon-containing secondary resources.

mineral deposits) while standardizing impurity tolerance thresholds for industrial adoption.

5.2.2. Energy-Efficient Process Innovation

Source-tailored low-energy processes are critical for sustainable scaling. Biomass conversion should optimize integrated pyrolysis, harnessing inherent organics as *in situ* reductants for simultaneous silicon reduction and carbon coating, to minimize external energy input while addressing residual ash impurities through gas-phase purification. For mineral and waste silicon, hybrid hydrometallurgy (selective acid leaching) coupled with molten salt electrolysis enables efficient metal removal and nanostructuring at reduced temperatures; however, waste stream management (e.g., pickling effluent detoxification via ion-exchange), and reactor design optimization remain key challenges. Emerging techniques like plasma-assisted purification and bioleaching (microbial Fe/Al dissolution) show promise for sub-100 nm silicon synthesis with $<1 \text{ kWh kg}^{-1}$ energy footprint, particularly for low-grade sources requiring minimal chemical consumption.

5.2.3. Biomimetic Structural Synergy

Maximizing intrinsic structural advantages will unlock transformative performance gains. Biomass silicon's hierarchical porosity and organic-inorganic interfaces offer pre-engineered ion-diffusion highways, while mineral silicon's ordered micro-nano architectures provide mechanically stable Li^+ transport networks. Strategically combining these innate topographies with atomic-scale modifications creates biomimetic electrodes where natural pore geometries accommodate volume change and engineered surfaces stabilize solid-electrolyte interphases. This "structure-function-chemical" triadic optimization, guided by multiscale computational modeling, will accelerate breakthroughs in areal capacity ($>5 \text{ mAh cm}^{-2}$) and extremely fast-charging capability, ultimately bridging laboratory innovation and gigawatt-h manufacturing.

Acknowledgements

This work was supported by the National Natural Science Foundation of China (52404423, 51874196), the Open Research Fund of Songshan Lake Materials Laboratory (2023SLABFK12), the Key Laboratory of Ionic Rare Earth Resources and Environment, Ministry of Natural Resources of the People's Republic of China (no. 2023IRERE205), and the Independent Research Project of State Key Laboratory of Advanced Special Steel, Shanghai Key Laboratory of Advanced Ferrometallurgy, Shanghai University (SKLASS2023-Z15).

Conflict of Interest

The authors declare no conflict of interest.

Author Contributions

Zihong Yu: formal analysis (equal); validation(lead); writing—original draft (equal). **Xinlin Peng:** formal analysis: equal; investigation(lead); writing—original draft (equal). **Jie Liu:** data curation (equal); formal analysis(supporting); software (equal). **Qiangchao Sun:** formal analysis(lead); resources (equal); supervision(supporting); visualization(lead); writing—review & editing (equal). **Zhifeng Xu:** methodology (equal); supervision(supporting). **Weifan Gao:** resources(supporting); software(supporting). **Hongwei Cheng:** conceptualization (lead); funding acquisition (lead); project administration (lead); resources (lead); supervision (lead).

Keywords: lithium-ion batteries • low cost • modification strategies • silicon-based anodes • silicon-containing resources

- [1] L. Zhang, S. Bi, X. Liu, Q. Sun, T. Hu, X. Lu, H. Cheng, *Energy Environ. Sci.* **2025**, *18*, 7555.
- [2] J. Li, F. Wang, C. Zhang, D. Dang, Q. Liu, J. Tan, *Batteries Supercaps* **2024**, *7*, e202400273.
- [3] L. Zhang, X. Liu, L. Chang, Q. Sun, X. Lu, H. Cheng, *Energy Storage Mater.* **2025**, *81*, 104508.
- [4] J. Liao, Q. Hu, J. Mu, X. He, S. Wang, D. Jiemin, C. Chen, *Chem. Commun.* **2019**, *55*, 13916.
- [5] X. Zhang, Q. Sun, C. Zhen, Y. Niu, Y. Han, G. Zeng, D. Chen, C. Feng, N. Chen, W. Lv, W. He, *Energy Storage Mater.* **2021**, *37*, 628.
- [6] L. Chang, S. Bi, J. Li, Q. Sun, X. Lu, H. Cheng, *ACS Nano* **2025**, *19*, 27424.
- [7] S. Chae, S.-H. Choi, N. Kim, J. Sung, J. Cho, *Angew. Chem., Int. Ed.* **2020**, *59*, 110.
- [8] C. Zhang, F. Wang, J. Han, S. Bai, J. Tan, J. Liu, F. Li, *Small Struct.* **2021**, *2*, 2100009.
- [9] L. Chang, H. Cheng, J. Li, L. Zhang, B. Zhang, L. Zheng, Q. Sun, J. Li, X. Lu, K. Zhao, *Nat. Commun.* **2025**, *16*, 6134.
- [10] L. Gao, C. Sun, D. Zhang, Y. An, Y. Yang, X. Bian, *Chem. Eng. J.* **2023**, *451*, 138410.
- [11] M. L. Philippot, D. Costa, G. Cardellini, L. De Sutter, J. Smekens, J. Van Mierlo, M. Messagie, *J. Energy Storage* **2023**, *60*, 106635.
- [12] M. Sun, T. Fang, H. Liu, Y. Li, W. Peng, F. Zhang, X. Fan, *Chem. Eng. J.* **2024**, *484*, 149359.
- [13] F. Wang, B. Wang, J. Li, B. Wang, Y. Zhou, D. Wang, H. Liu, S. Dou, *ACS Nano* **2021**, *15*, 2197.
- [14] L. Li, R. Qin, R. Zhan, C. Tu, X. Liu, L. Liu, L. Deng, *J. Energy Storage* **2024**, *98*, 113196.
- [15] P. Qiu, M. Cui, H. Gan, L. Li, Y. Xia, J. Sun, W. Zhu, *Carbon* **2025**, *233*, 11905.
- [16] W. He, W. Xu, Z. Li, Z. Hu, J. Yang, G. Qin, W. Teng, T. Zhang, W. Zhang, Z. Sun, X. Yu, *Adv. Sci.* **2025**, *12*, 2407540.
- [17] H. Ahmed, G. S. dos Reis, P. Molaiyan, A. Lähde, U. Lassi, *Prog. Energy* **2025**, *7*, 022003.
- [18] F. Wang, Y. Wang, Z. Liu, C. Zhang, L. Li, C. Ye, J. Liu, J. Tan, *Adv. Energy Mater.* **2023**, *13*, 2301456.
- [19] Z. Yan, J. Jiang, Y. Zhang, D. Yang, N. Du, *Mater. Today Nano* **2022**, *18*, 100175.
- [20] F.-H. Du, K.-X. Wang, J.-S. Chen, *J. Mater. Chem. A* **2016**, *4*, 32.
- [21] X. Liu, X. Zhu, D. Pan, *R. Soc. Open Sci.* **2018**, *5*, 172370.
- [22] P. Li, G. Zhao, X. Zheng, X. Xu, C. Yao, W. Sun, S. X. Dou, *Energy Storage Mater.* **2018**, *15*, 422.
- [23] F. Ozanam, M. Rosso, *Mater. Sci. Eng., B* **2016**, *213*, 2.
- [24] Y. Jin, B. Zhu, Z. Lu, N. Liu, J. Zhu, *Adv. Energy Mater.* **2017**, *7*, 1700715.
- [25] C. Sun, J. Pan, X. Fu, D. Ma, L. Cui, W. Yao, C. Jiao, Y. Xu, H. Hao, M. Li, A. Du, Q. Wang, *Mater. Today Sustainability* **2024**, *27*, 100898.
- [26] K. Sun, X. Li, Z. Zhang, K. Fu, X. Xiao, L. Gong, P. Tan, *Energy Storage Mater.* **2024**, *66*, 103216.
- [27] P. Xu, D. Guo, X. Wang, Y. Cao, Z. Zhang, X. Lin, Z. Su, Q. Huang, F. Wu, M. Zhang, *Mater. Today Energy* **2025**, *48*, 101766.
- [28] Z. You, C. Lin, P. Zheng, J. Li, Q. Feng, J. Tao, Y. Zheng, Y. Lin, Z. Huang, J. Li, *Small* **2025**, *21*, 2407215.
- [29] K. Min, K. Kim, H. An, Y. Go, Y. Lee, D. Lim, S.-H. Baeck, *J. Power Sources* **2022**, *543*, 231849.
- [30] J. Li, F. Wang, L. Xue, D. Dang, Q. Liu, C. Ye, C. Zhang, J. Tan, *Appl. Energy* **2025**, *390*, 125820.
- [31] Y. Gao, S. Song, F. He, X. Kong, Z. Xiao, X. Cui, L. Cao, Y. Zhang, Z. Liu, P. Yang, *Small* **2024**, *20*, 2406489.
- [32] J. Li, S. Wang, F. Wang, Z. Liu, Z. Tang, W. Zhang, D. Dang, C. Pan, Q. Liu, C. Zhang, *Mater. Chem. Front.* **2025**, *9*, 1896.
- [33] K. Chen, Y. Tan, K. Wang, J. Niu, Z. Y. Chen, *Electrochim. Acta* **2022**, *401*, 139497.
- [34] W. U. Rehman, H. Wang, R. Z. A. Manj, W. Luo, J. Yang, *Small* **2021**, *17*, 1904508.
- [35] K. Yu, H. Zhang, H. Qi, J. Liang, C. Liang, *New J. Chem.* **2018**, *42*, 19811.
- [36] C. Zhang, X. Cai, W. Chen, S. Yang, D. Xu, Y. Fang, X. Yu, *ACS Sustainable Chem. Eng.* **2018**, *6*, 9930.
- [37] X.-Y. Yue, A. Abulkeme, X.-L. Li, Q.-Q. Qiu, F. Wang, X.-J. Wu, Y.-N. Zhou, *J. Power Sources* **2019**, *410*, 132.
- [38] T. Shen, Z. Yang, Y. Chen, J. Mei, J. Xu, *J. Solid State Electrochem.* **2023**, *27*, 2407.
- [39] S. Mei, Y. Liu, J. Fu, S. Guo, J. Deng, X. Peng, X. Zhang, B. Gao, K. Huo, P. K. Chu, *Appl. Surf. Sci.* **2021**, *563*, 150280.
- [40] N. Ding, J. Xu, Y. Yao, G. Wegner, I. Lieberwirth, C. Chen, *J. Power Sources* **2009**, *192*, 644.
- [41] Y. Wang, S. Wang, L. Xue, F. Wang, F. Qi, Y. Zhou, C. Zhang, J. Tan, H. Pan, C. Ye, *ACS Nano* **2025**, *19*, 1660.
- [42] I. Kovalenko, B. Zdyrko, A. Magasinski, B. Hertzberg, Z. Milicev, R. Burtovyy, I. Luzinov, G. Yushin, *Science* **2011**, *334*, 75.
- [43] C. K. Chan, H. Peng, G. Liu, K. McIlwrath, X. F. Zhang, R. A. Huggins, Y. Cui, *Nat. Nanotechnol.* **2008**, *3*, 31.
- [44] M. Ge, J. Rong, X. Fang, A. Zhang, Y. Lu, C. Zhou, *Nano Res.* **2013**, *6*, 174.
- [45] Y. Xu, Y. Zhu, C. Wang, *J. Mater. Chem. A* **2014**, *2*, 9751.
- [46] W.-J. Yu, C. Liu, P.-X. Hou, L. Zhang, X.-Y. Shan, F. Li, H.-M. Cheng, *ACS Nano* **2015**, *9*, 5063.
- [47] Z. Zhou, L. Pan, Y. Liu, X. Zhu, X. Xie, *Chin. Chem. Lett.* **2019**, *30*, 610.
- [48] R. Gao, J. Tang, K. Zhang, K. Ozawa, L.-C. Qin, *Nano Energy* **2020**, *78*, 105341.
- [49] Y. D. Cao, J. C. Bennett, R. A. Dunlap, M. N. Obrovac, *Chem. Mater.* **2018**, *30*, 7418.
- [50] H. Liu, Y. G. Long, Y. Chen, Z. G. Wang, C. Zhang, R. Z. Hu, X. Zhang, P. Yu, *ACS Appl. Mater. Interfaces* **2021**, *13*, 57317.
- [51] J. Cao, X. Yan, D. Li, L. Hu, T. Chen, W. Gao, W. Song, X. Xia, Y. Xia, W. Zhang, H. Huang, *Chem. Eng. J.* **2025**, *504*, 159049.
- [52] S. U. Pesulo, L. A. September, N. Kheswa, N. S. Seroka, L. Khotseeng, *Processes* **2024**, *12*, 1817.
- [53] J. Cui, Y. Cui, S. Li, H. Sun, Z. Wen, J. Sun, *ACS Appl. Mater. Interfaces* **2016**, *8*, 30239.
- [54] Y. Feng, L. Liu, X. Liu, Y. Teng, Y. Li, Y. Guo, Y. Zhu, X. Wang, Y. Chao, *Electrochim. Acta* **2020**, *359*, 136933.
- [55] Y.-C. Zhang, Y. You, S. Xin, Y.-X. Yin, J. Zhang, P. Wang, X.-s. Zheng, F.-F. Cao, Y.-G. Guo, *Nano Energy* **2016**, *25*, 120.

- [56] K. Askaruly, N. Idrissov, A. Abdisattar, S. Azat, Z. Kuli, M. Yeleuov, F. Malchik, C. Daulbayev, Y. Yszhan, B. Sarsembayeva, S. Nysanbayeva, *Diamond Relat. Mater.* **2024**, *149*, 111631.
- [57] H. Wei, D. Xu, W. Chen, X. Liu, Z. Zhang, L. Dai, H. Hu, X. Yu, *Appl. Surf. Sci.* **2022**, *584*, 152580.
- [58] J. Liu, P. Kopold, P. A. van Aken, J. Maier, Y. Yu, *Angew. Chem., Int. Ed.* **2015**, *54*, 9632.
- [59] M. Sun, J. Ma, M. Xu, H. Yang, J. Zhang, C. Wang, *ACS Omega* **2022**, *7*, 15123.
- [60] K. Thangaian, T. Ericson, P. E. Vullum, P. Alonso-Sánchez, A. C. Svarerud, A. M. Svensson, F. Vullum-Bruer, M. Hahlin, M. V. Blanco, *J. Power Sources* **2025**, *641*, 236837.
- [61] Y. Lin, Z. Zha, X. Hui, T. Hu, U. Lassi, Z. Chen, R. Ma, Z. Wu, *Mater. Today Chem.* **2024**, *36*, 101925.
- [62] Y. Ouyang, Y. Song, J. Wang, W. Li, A. Pan, C. Han, *Chem. Eng. J.* **2025**, *507*, 160699.
- [63] Q. Chen, S. Wei, R. Zhu, J. Du, J. Xie, H. Huang, J. Zhu, Z. Guo, *Chem. Commun.* **2023**, *59*, 14297.
- [64] H. Ruan, S. Guo, L. Zhang, Y. Liu, L. Li, Y. Huang, S. Gao, Y. Tian, *Ceram. Int.* **2022**, *48*, 17510.
- [65] F. Di, N. Wang, L. Li, X. Geng, H. Yang, W. Zhou, C. Sun, B. An, *J. Alloys Compd.* **2021**, *854*, 157253.
- [66] F. Wang, W. Liu, P. Li, Z. Guan, W. Li, D. Wang, *Small* **2024**, *20*, 2311334.
- [67] Z. Lin, P. Sun, C. Zhou, Z. Z. Fang, *ACS Omega* **2025**, *10*, 473.
- [68] W.-S. Kim, Y. Hwa, J.-H. Shin, M. Yang, H.-J. Sohn, S.-H. Hong, *Nanoscale* **2014**, *6*, 4297.
- [69] L. Hou, B. Xing, W. Kang, H. Zeng, H. Guo, S. Cheng, G. Huang, Y. Cao, Z. Chen, C. Zhang, *Appl. Clay Sci.* **2022**, *218*, 106418.
- [70] H. Wang, W. Tang, L. Ni, W. Ma, G. Chen, N. Zhang, X. Liu, R. Ma, *J. Phys. Chem. Solids* **2020**, *137*, 109227.
- [71] L. Shen, K. Sun, F. Xi, Z. Jiang, S. Li, Y. Wang, Z. Tong, J. Lu, W. Ma, M. A. Green, X. Hao, *Energy Environ. Sci.* **2025**, *18*, 4348.
- [72] Y. Zhang, Z. Zhang, W. Chen, X. Zhang, Z. Guan, *Mater. Today Commun.* **2024**, *40*, 109322.
- [73] C. Zhang, J. Li, Y. Feng, G. Du, Y. Liu, Y. Wang, Y. Wang, Z. Wu, P. Yang, A. K. Nanjundan, K. Yang, X. Zhu, L. Zhang, *ACS Sustainable Chem. Eng.* **2024**, *12*, 14099.
- [74] N. Akhil, M. Srikanth, C. Ying, S. Neeraj, H. Qi, R. M. Mokhlesur, *Energy Mater.* **2024**, *4*, 400064.
- [75] X. Liu, Q. Zhang, Y. Zhu, J. Zhao, J. Chen, H. Ye, H. Wei, Z. Liu, *Silicon* **2022**, *14*, 7983.
- [76] Y. Jiang, Y. Zhang, X. Yan, M. Tian, W. Xiao, H. Tang, *Chem. Eng. J.* **2017**, *330*, 1052.
- [77] Q. Bao, Y.-H. Huang, C.-K. Lan, B.-H. Chen, J.-G. Duh, *Electrochim. Acta* **2015**, *173*, 82.
- [78] C.-Y. Chou, J.-R. Kuo, S.-C. Yen, *ACS Sustainable Chem. Eng.* **2018**, *6*, 4759.
- [79] W. Kang, J.-C. Kim, J. H. Noh, D.-W. Kim, *ACS Sustainable Chem. Eng.* **2019**, *7*, 15329.
- [80] M. Choi, J.-C. Kim, D.-W. Kim, *Sci. Rep.* **2018**, *8*, 960.
- [81] S. Sudarman, T. Andriyani, M. Taufik, *Mater. Sci. Energy Technol.* **2024**, *7*, 1.
- [82] W. C. Cho, H. J. Kim, H. I. Lee, M. W. Seo, H. W. Ra, S. J. Yoon, T. Y. Mun, Y. K. Kim, J. H. Kim, B. H. Kim, J. W. Kook, C.-Y. Yoo, J. G. Lee, J. W. Choi, *Nano Lett.* **2016**, *16*, 7261.
- [83] W. Tao, C. Xu, P. Gao, K. Zhang, X. Zhu, D. Wu, J. Chen, *J. Colloid Interface Sci.* **2024**, *669*, 902.
- [84] Q. Chen, S. Liu, R. Zhu, D. Wu, H. Fu, J. Zhu, H. He, *J. Power Sources* **2018**, *405*, 61.
- [85] J. Ryu, D. Hong, M. Shin, S. Park, *ACS Nano* **2016**, *10*, 10589.
- [86] N. Wan, L. Wang, S.-Y. Li, L. Shen, F.-S. Xi, J.-J. Lu, Z.-Q. Tong, X.-H. Chen, W.-H. Ma, *Small* **2025**, 2412705, <https://doi.org/10.1002/smll.202412705>.
- [87] Y. Zhang, H. Ma, C. Yu, X. Feng, *Mater. Lett.* **2023**, *331*, 133469.
- [88] B. Wang, Y. Guo, J. Du, Q. Li, X. Zhang, Y. Bao, J. Liu, D. Wang, J. Ma, Y. Zhou, *Ionics* **2023**, *29*, 5099.
- [89] Z. Zhang, F. Xi, S. Li, X. Wan, W. Ma, X. Chen, Z. Chen, R. Deng, J. Ji, H.-J. Fan, C. Chong, *Mater. Today Energy* **2021**, *20*, 100671.
- [90] W. Chen, H. Liu, S. Kuang, H. Huang, T. Tang, M. Zheng, Y. Fang, X. Yu, *Carbon* **2021**, *179*, 377.
- [91] M. Gautam, G. K. Mishra, M. Furquan, K. Bhawana, D. Kumar, S. Mitra, *Chem. Eng. J.* **2023**, *472*, 144916.
- [92] X. Kong, Z. Xi, Y. Jiang, S. Li, X. Chen, J. Zhang, L. Wang, Z. Wan, A. Pan, *Chem. Eng. J.* **2023**, *477*, 147178.
- [93] C. Padwal, H. D. Pham, L. T. M. Hoang, S. Mundree, D. Dubal, *Sustainable Mater. Technol.* **2023**, *35*, e00547.
- [94] Q. Aini, P. B. Persada, M. H. R. Pasha, N. H. Hawari, A. Sumboja, *ACS Sustainable Chem. Eng.* **2024**, *12*, 14296.
- [95] X. Guo, W. Li, P. Geng, Q. Zhang, H. Pang, Q. Xu, *J. Colloid Interface Sci.* **2022**, *606*, 784.
- [96] X. Guo, W. Li, Q. Zhang, Y. Liu, G. Yuan, P. Braunstein, H. Pang, *Chem. Eng. J.* **2022**, *432*, 134413.
- [97] J. Cui, H. Zhang, Y. Liu, S. Li, W. He, J. Hu, J. Sun, *Electrochim. Acta* **2020**, *334*, 135619.
- [98] W. Chen, D. Xu, S. Kuang, Z. Wu, H. Hu, M. Zheng, X. Yu, *J. Power Sources* **2021**, *489*, 229459.
- [99] Z. Pang, X. Xiong, F. Tian, X. Zhang, F. Wang, X. Xia, G. Li, C. Sun, S. Wang, X. Yu, Q. Xu, X. Zou, X. Lu, *ACS Sustainable Chem. Eng.* **2024**, *12*, 7200.
- [100] K. Wang, Z. Liu, S. Mu, H. Shi, M. Zhou, C. Yuan, S. Lu, Z. Ni, G. Tian, *J. Alloys Compd.* **2025**, *1022*, 180063.
- [101] Y. Li, L. Liu, X. Liu, Y. Feng, L. Yu, Z. He, X. Cui, M. Zhang, Y. Zhu, X. Wang, *Ionics* **2022**, *28*, 151.
- [102] S. Liu, Q. Zhang, H. Yang, D. Mu, A. Pan, S. Liang, *Minerals* **2018**, *8*, 180.
- [103] X. Tang, G. Wen, Y. Song, *J. Alloys Compd.* **2018**, *739*, 510.
- [104] S. Wei, Q. Chen, R. Zhu, J. Du, J. Xie, H. Fu, T. Xiong, H. Liu, J. Zhu, *Appl. Clay Sci.* **2024**, *254*, 107388.
- [105] X. Huang, Y. Ding, K. Li, X. Guo, Y. Zhu, Y. Zhang, Z. Bao, *J. Power Sources* **2021**, *496*, 229833.
- [106] Q. Yu, J. Liu, Y. Liang, T. Liu, Y. Zheng, Z. Lai, X. Liu, J. Chen, Q. Zhang, X. Li, *Electrochim. Acta* **2022**, *422*, 140515.
- [107] W. Liu, J. Liu, M. Zhu, W. Wang, L. Wang, S. Xie, L. Wang, X. Yang, X. He, Y. Sun, *ACS Appl. Mater. Interfaces* **2020**, *12*, 57055.
- [108] Y. Li, G. Chen, H. Wu, H. Ding, C. Zhang, L. Huang, X. Luo, *Appl. Surf. Sci.* **2023**, *634*, 157651.
- [109] Y. Ma, A. Huang, Y. Li, H. Jiang, W. Zhang, L. Zhang, L. Li, S. Peng, *J. Alloys Compd.* **2022**, *890*, 161792.
- [110] Y. Li, G. Chen, W. Liu, C. Zhang, L. Huang, X. Luo, *Waste Manage.* **2023**, *156*, 22.
- [111] A. Su, J. Li, J. Dong, D. Yang, G. Chen, Y. Wei, *Small* **2020**, *16*, 2001714.
- [112] Q. Li, J. Zhao, W. Yao, C. Yu, X. Ding, *Mater. Chem. Phys.* **2023**, *305*, 128015.
- [113] Y. Zhang, W. Tang, H. Gao, M. Li, H. Wan, X. Kong, X. Liu, G. Chen, Z. Chen, *ACS Nano* **2024**, *18*, 15671.
- [114] L. Wang, X. Zheng, Y. Yu, F. Xi, S. Li, W. Ma, Z. Tong, X. Wan, *J. Electroanal. Chem.* **2024**, *952*, 117942.
- [115] T. K. Pham, J. H. Shin, N. C. Karima, Y. S. Jun, S.-K. Jeong, N. Cho, Y.-W. Lee, Y. Cho, S. N. Lim, W. Ahn, *J. Power Sources* **2021**, *506*, 230244.
- [116] K. J. Nyamtara, J. K. Song, N. C. Karima, S. H. Kim, M. C. Nguyen, T. P. M. Duong, K. J. Lee, W. Ahn, *J. Alloys Compd.* **2024**, *976*, 173229.
- [117] B. Sreenarayanan, M. Vicencio, S. Bai, B. Lu, O. Mao, S. Adireddy, W. Bao, Y. S. Meng, *J. Power Sources* **2023**, *578*, 233245.
- [118] T. Mu, B. Shen, S. Lou, Z. Zhang, Y. Ren, X. Zhou, P. Zuo, C. Du, Y. Ma, H. Huo, G. Yin, *Chem. Eng. J.* **2019**, *375*, 121923.
- [119] C. Zhang, Q. Ma, M. Cai, Z. Zhao, H. Xie, Z. Ning, D. Wang, H. Yin, *Waste Manage.* **2021**, *135*, 182.

Manuscript received: July 22, 2025

Revised manuscript received: August 25, 2025

Version of record online: